TEL AVIV UNIVERSITY
RAYMOND AND BEVERLY SACKLER
FACULTY OF EXACT SCIENCES
SCHOOL OF PHYSICS & ASTRONOMY

אוניברסיטת תל-אביב
הפקולטה למדעים מדויקים
ע"ש ריימונד ובברלי סאקלר
בית הספר לפיסיקה ואסטרונומיה

Directed Stochastic Motion

by

Oded Farago

Thesis submitted in partial
fulfillment of the requirements
for the M.Sc. degree
at Tel-Aviv University
School of Physics and Astronomy

The research work for this thesis has been
carried out under the supervision of
Professor Yacov Kantor

May 1996

Acknowledgment

It is a great pleasure for me to thank my supervisor, Professor Yacov Kantor, for his guidance, patience and support. I benefited a lot from his vast knowledge, experience and deep physical intuition.

The model introduced in this work was first formulated and studied by Professor Marko V. Jaric. I am indebted to him for interesting discussions.

I would also like to thank my colleagues Ravi Sachidanandam, Eilon Brenner, Haim Diamant and Itamar Borukhov for assistance, whenever needed.

Last, but not least, thanks to my parents and Zahit for their generous encouragement and moral support.

Contents

Abstract

We study a particle moving within a one dimensional potential field composed of a set of equally spaced oscillating potential barriers. The velocity and the height of the barriers change periodically with time. We follow the motion of a particle which goes through a set of collisions with the barriers, thus changing its velocity. This motion is asymmetric and a net directed motion is detected in the system. The amplitude of the barrier's height is chosen to be the control parameter of the problem.

A 2-dimensional map describes the dynamics. We prove that the map is a one-to-one area-preserving transformation of the phase space into itself. Iterations of the map are performed and the corresponding "return-maps" are constructed to give pictures of the related phase spaces, which, in turn, are used to study the features of the particle's motion. Two types of motion in phase space are revealed, depending on the initial conditions: A stochastic motion which covers ergodicaly a "stochastic sea", and a regular motion over closed curves, located inside chains of islands which are embedded in the stochastic sea.

A combination of analytical and numerical studies shows that the asymmetry of the dynamics is expressed in two ways: A difference between the maximal speeds which the particle can gain in both directions and the existence of asymmetrical chains of islands in the phase space which correspond to a highly efficient regular motion.

The appearance of these chains of islands is also related to the phenomenon of pseudo KAM boundaries, which we discuss.

1 General Introduction

1.1 Chaotic Systems

The evolution of many physical systems is given in terms of differential or difference equations, and is thus completely determined by initial conditions. This kind of behavior is called *deterministic*. For many years, it was believed that "simple" equations, for example, first or second order differential equations consisting of smooth well defined functions, lead to "simple", regular outcomes. However, in 1892, the French mathematician, H. Poincarè [1], showed that some systems, whose time evolution is governed by Hamilton's equations, may exhibit a rather complicated, nowadays called *chaotic*, behavior. Following Poincarè, many scientists investigated this kind of dynamics. Yet, it took 70 to realize that chaos can be found in real physical systems. It was the meteorologist E.N. Lorenz [2] who found that even a simple set of three coupled, first order, nonlinear equations, can lead to irregular dynamics. Lorenz found that the solutions resulting from very close initial conditions, diverge rapidly with time, and soon lose any similarity. This feature is called *"sensitive dependence on initial conditions"*.

The same features that characterize Lorenz' system (irregular behavior and fast divergence of nearby trajectories) were detected since then in many other systems. Deterministic nonlinear physical systems whose dependence on initial conditions is sensitive, and which behave in an irregular complicated way are called chaotic. The origin of chaos is the nonlinearity of the system. The sensitive dependence on initial conditions can be quantified by means of characteristic exponents which measure the rate of divergence of nearby trajectories. It makes the prediction of long time behavior impossible in chaotic systems, since both the determination of initial conditions and numerical calculations of their evolution in time, have a finite precision, and errors increase exponentially fast. The second characteristic of chaotic behavior, namely the irregularity of the dynamics, is however more difficult to define. There are several ways, both theoretical and experimental, to distinguish between regular and irregular behavior in physical systems and, in particular, to detect the transition between them (see [3], chapter 1).

In the last two decades, chaos has been found in a wide variety of systems in many fields of science like physics, chemistry, biology, economy, etc. The fast progress in the research of chaotic systems in recent years can be mainly attributed to the availability of more powerful computers and the development of better experimental techniques. Parallel to that, new theoretical results have been established to provide some universal concepts in this interdisciplinary subject called chaos.

1.2 Motion Rectification

According to the second law of thermodynamics, heat cannot be converted into work in an isothermal system [4]. A particle placed in a thermal bath will diffuse randomly in the system without displaying any net drift velocity. Even if an asymmetric, but homogeneous on the macroscopic scale, potential is applied in the system, a directed motion will not be induced. Consider a particle diffusing in an asymmetric potential depicted in Fig. 1, the particle will spend most of the time near one of the minima. Occasionally, it will hop from one well to its neighbor. However, in the absence of large scale gradients, an equilibrium situation will be achieved, with no net currents of particles. Similar behavior can be expected in a random potential.

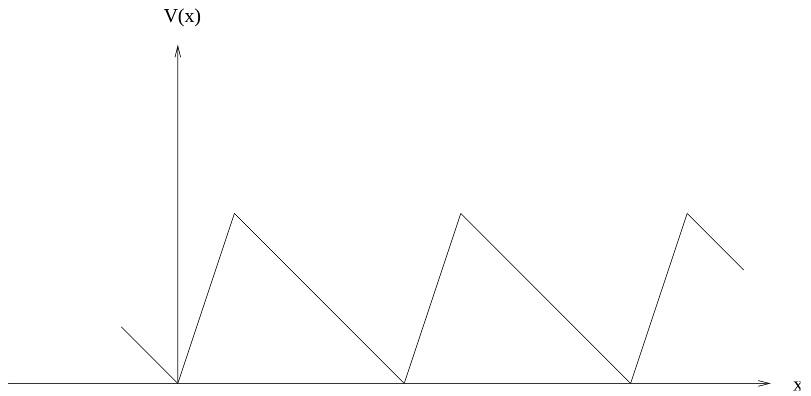

Figure 1: An asymmetric, but homogeneous on the large scale, potential.

Recently it has been shown, both theoretically and experimentally, that the application of an external time dependent force can induce a net directed motion in the system, even if the applied force is an oscillatory force of zero time average [5]–[12]. The basic idea is that since the potential well is asymmetric, the same force, applied for the same interval of time, may "pull" the particle out of the well in one direction, but not in the other. Directed motion can also be induced without the application of any external force, provided the thermal noise is colored, i.e., time correlated (it can still however have zero time average), or if the asymmetric potential is switched on and off. Such rectification processes are interesting because they can lead to the generation of microscopic pumping and separation techniques in which particle currents are induced with some characteristic velocity. They also may provide some insight into the mechanism of *protein motors*.[1]

1.3 Deterministic Dynamics vs. Statistical Kinetics

Most of the papers mentioned above, deal with systems out of equilibrium. The kinetics of these systems are handled using statistical-mechanical "tools" like the Langevin equations or their related Fokker-Planck equations, which do not describe the actual motion of the particle, but refer to the distribution density in real or phase space. On the other hand, there are some cases when one is able to write the particle's equations of motion. In these cases the dynamics are deterministic. They might however be chaotic and therefore we are usually not interested in the description of some specific trajectory of the particle, but in the general properties common to a large group of trajectories.

This is the subject of this work: We will investigate the motion of a particle in an asymmetric potential which is periodic both in time and space. Unlike other papers, we will deal with the deterministic case. The *stochastic* deterministic dynamical system will be introduced in the next chapter.[2] We will try to detect the existence of a drift velocity (which we hope to find independent of initial conditions), and show its dependence on the parameters which characterize the periodic potential. The framework of our discussion is therefore the field of chaotic deterministic dynamics.

It should be stressed that the choice between deterministic and statistical approaches, is not a matter of a choice, but should be derived from the problem in question. If, for example, the particle is diffusing due to interaction with thermal noise, then a statistical approach is applied. On the other hand, if thermal noise is negligible in comparison to external forces, then a deterministic approach can be used.

[1] Protein motors are molecules, such as kinesins and dynesins, which participate in transport processes inside eukariotic cells (the cells in all multicellular organisms). These motors "walk" on filaments made of polymerized proteins, such as tubulin and actin, which serve as the asymmetric potential in this problem. Time correlations might arise from the statistics of the "attachments" of ATP (Adenosine Triposphate), the source of chemical energy, to the motors.

[2] The terms stochastic and chaotic are used interchangeably to describe the same kind of dynamics. The term "chaotic" is commonly used to describe the motion in dissipative systems, while the term "stochastic" usually refers to non-dissipative (Hamiltonian) systems.

2 Introduction of the Dynamical System

2.1 What is a Map?

The dynamical system under investigation in this work will be introduced in the next section. The dynamics of deterministic systems can be described in terms of a set of N discrete equations of motion: $\vec{z}_{n+1} = T(\vec{z}_n)$, where $\vec{z}_n$ is the N-dimensional vector $\vec{z} = \begin{pmatrix} \alpha_1 \\ \vdots \\ \alpha_N \end{pmatrix}$ at time $t = n\tau$ and T is the time-evolution operator. Such a system of equations of motion, which gives $\vec{z}_{n+1}$ in terms of $\vec{z}_n$ is called a *map* (or a *mapping* or an *iterative map*). Describing the evolution of a dynamical system using a map has few advantages over the description through a set of differential equations: $\dot{\vec{z}} = f(\vec{z})$. Maps are usually easier to compute than differential equations which require the use of numerical schemes for their solution. The use of numerical schemes (which are mappings themselves), might give rise to problems of instability. The instability is frequently related to the use of certain schemes and does not represent features of the motion itself. Such "technical problems" do not appear while using iterative maps.[1] Another great advantage of the use of maps comes from the relative simplicity of the description of the motion they yield. One usually finds it easier to visualize the *trajectory* $\{T^n(\vec{z}_0)$; n integer$\}$, composed of a set of discrete points, than following the trajectory $\vec{z}(t)$, which is a continuous curve in the *phase space*.

The continuous description $\vec{z}(t)$ can be converted into a discrete one by using the method of *Poincarè sections*. Following $\vec{z}(t)$ in the N-dimensional phase space, one can look at the intersections of the trajectory with the surface $\alpha_N = \text{const}$ (α_N is the N-th component of the vector $\vec{z}$). These intersections construct a *return* (Poincarè) *map* which gives an alternative discrete description of the motion. Moreover, we have thus reduced the dimensionality of the problem from N to $N-1$. For example, consider a *Hamiltonian system*, i.e., such that the equations of motion are the Hamilton's equations. As the phase space set of coordinates one usually chooses the N coordinates of the position $q_1 \dots q_N$ and the N conjugate coordinates of momenta $p_1 \dots p_N$. Another frequently used set consists

[1] A trajectory computed using an iterative map can also deviate from the "real" trajectory because of the finite precision of numerical computations. This deviation can be (exponentially) amplified in time. However, this then simply reflects the chaotic unstable nature of the motion. By "technical problems" we refer to the instability of the numerical scheme itself, which is an additional problem in solving numerically differential equations.

of the N coordinates of action $I_1 \ldots I_N$ and the N conjugate angles $\Theta_1 \ldots \Theta_N$.[2] Energy conservation and the use of Poincarè section bring us into a discrete problem of motion in a $2N-2$ dimensional phase space. It is convenient to visualize the obtained trajectory by projecting this $2(N-1)$-dimensional phase space on the $(N-1)$ 2-dimensional planes $((q_i, p_i)\ ;\ 1 \leq i \leq N-1)$.

It should be noted that the time itself can be one of the coordinates of the phase space. The set of equations of motion $\dot{\vec{z}} = f(\vec{z}, t)$ ($\vec{z}_{n+1} = T(\vec{z}_n, t_n)$ in the discrete case) can be written in the form $\dot{\vec{w}} = f(\vec{w})$, where $\vec{w} = \begin{pmatrix} \alpha_1 \\ \vdots \\ \alpha_N \\ t \end{pmatrix}$ and the "new" time is $\xi(t) = t$. Thus, by extending the phase space by an additional degree of freedom, one replaces a set of equations including time dependent functions, by a set of equations in which the functions are time independent. (Dealing with Hamiltonian systems, one extends the phase space by adding a pair of (conjugate) coordinates: $q_{N+1} = t\ ;\ p_{N+1} = -\mathcal{H}$, where $\mathcal{H}$ is the Hamiltonian.) We should not therefore be surprised to find systems in which the time is one of the coordinates of the phase space, as is the one discussed in this work.

2.2 The Potential Field and the Dynamics

We now introduce the problem under investigation in this work and explain why are the dynamics described in this problem asymmetric. We consider a particle moving in a potential field. This potential field is periodic both in time and space: $U(x+mL, t+l\tau) = U(x,t)$, where m and l are integers. It is composed of an infinite set of equally spaced potential barriers of an infinitesimal width each, described by:

$$U(x,t) \quad = \quad H(t) \sum_{m=-\infty}^{+\infty} \delta_{x-\tilde{x}(t), mL} \ ,$$

where δ is the Kronecker delta. The barriers oscillate and the quantity $\tilde{x}(t)$ describes the motion of the m-th ($m = 0, \pm 1, \ldots$) barrier around the point $x = mL$ (L is the spacing between the barriers). This motion is periodic in time with period τ, i.e., $\tilde{x}(t) = x_b f(t)$,

[2] $\vec{q}$ and $\vec{p}$, or any other set of $2N$ coordinates of Hamiltonian system, are said to be *conjugate* if they satisfy: $\dot{p}_i = -\frac{\partial \mathcal{H}}{\partial q_i}$ and $\dot{q}_i = \frac{\partial \mathcal{H}}{\partial p_i}$, where $\mathcal{H}$ is the Hamiltonian.

where $f(t+\tau) = f(t)$; f is normalized so that $\max|f(t)| = 1$ and x_b is the amplitude of the motion which is much smaller than L. The velocity of the barrier is:

$$v(t) = \dot{\tilde{x}}(t) = v_b g(t), \tag{2.1}$$

where, again, $g(t+\tau) = g(t)$, $\max|g(t)| = 1$ and v_b is the maximal velocity of the barrier. The height of the barrier, $H(t)$, which is also periodic in time with period τ, will be given by:

$$H(t) = H_0[1 + g(t)]. \tag{2.2}$$

As a periodic time dependent function we choose

$$g(t) = \sin(2\pi t), \tag{2.3}$$

which implies: $f(t) = -\cos(2\pi t)$, $v_b = 2\pi x_b$ and $\tau = 1$. We shall use dimensionless units throughout this work. The period of the barriers' motion, $\tau = 1$, will serve as the basic time unit. As an arbitrary selection of the length unit we set $x_b = \frac{1}{4\pi}$. Fig. 2 depicts schematically the potential field.

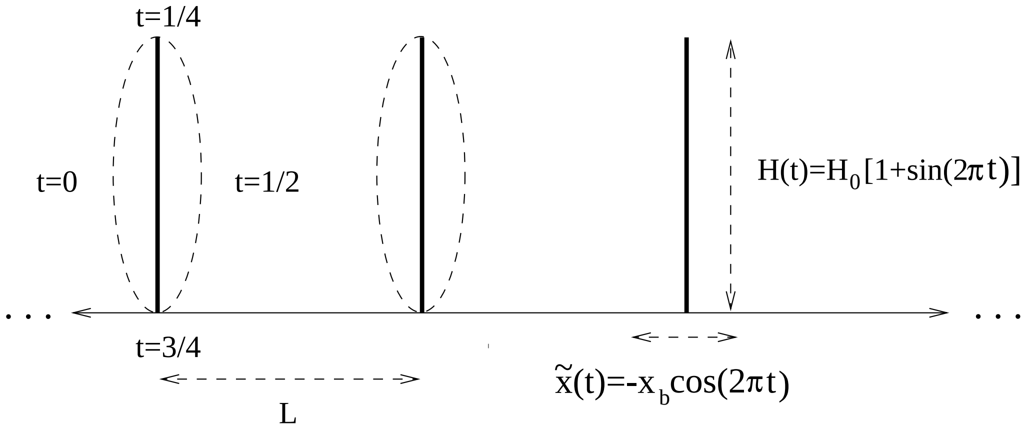

Figure 2: The potential field discussed in this work. It consists of a set of equally spaced potential barriers of zero width. The distance between neighboring barriers is L. The periodic function $\tilde{x}(t) = -x_b\cos(2\pi t)$ describes the position of the m-th barrier ($m = 0, \pm 1, \ldots$) around its mean position $x = mL$ and $H(t) = H_0[1+\sin(2\pi t)]$ describes the barriers' height. The ellipses depict the height of the barriers as a function of their spatial position.

A particle moves freely in this potential field between the barriers, occasionally colliding with one of them. It can either cross or be reflected from the barrier. This depends on (1) the height of the barrier, $H(t)$, at the moment of impact, (2) the velocity of the barrier, $v(t)$, at the moment of impact and (3) the velocity of the particle, V. In the reference frame of the moving barrier, the particle hits the non-moving barrier with a velocity

$V - v(t)$. The condition for crossing the barrier is that the kinetic energy of the particle in the reference frame of the barrier exceeds the height of the potential barrier. Taking the mass of the particle $m = 1$ (the basic mass unit), this condition can be expressed as follows: $|V - v(t)| > \sqrt{2H(t)}$ for crossing the barrier, while $|V - v(t)| \leq \sqrt{2H(t)}$ for being reflected from it. Since the velocity of the barriers is a periodic function with period $\tau = 1$, it is convenient to talk about the time t, taken modulus 1 and called the *phase*. It should be noted that the velocities of both the particle and the barrier are positive (negative) when the motion is from left to right (right to left). At the moment of impact $V > v(t)$ ($V < v(t)$); using Eqs. (2.1)–(2.3), the condition for crossing the barrier is given by

$$|V| > \begin{cases} \sqrt{2H_0[1+\sin(2\pi t)]} \pm v_b \sin(2\pi t) & \text{for } 0 < t \leq \frac{1}{2}, \\ \sqrt{2H_0[1-\sin(2\pi(t-\frac{1}{2}))]} \mp v_b \sin(2\pi(t-\frac{1}{2})) & \text{for } \frac{1}{2} < t \leq 1, \end{cases} \tag{2.4}$$

where the upper (lower) sign corresponds to situations of collision at a barrier from the left (right).

From Eq. (2.4), one can easily see the source of asymmetry between the two directions. For $0 < t < \frac{1}{2}$, when the barrier is moving from left to right ($v(t) > 0$) the height of the barrier satisfies $H_0 < H(t) < 2H_0$. For $\frac{1}{2} < t < 1$, when the barrier is moving from right to left ($v(t) < 0$), with the speed as at $t - \frac{1}{2}$, the height of the barrier is $0 < H(t) < H_0$. The motion of the barriers in a certain direction at each of the two halves of a period breaks the symmetry, since the condition for crossing a barrier depends on the relative velocity between the particle and the barrier. However, since $v(t) = -v(t - \frac{1}{2})$, there is an "inverse" symmetry between the two halves. It is the difference between the heights of the barriers in the two halves, that is, the fact that $H(t) \neq H(t - \frac{1}{2})$, which breaks this symmetry and causes the asymmetry of the dynamics (see Fig. 3).

Let V_n be the velocity of the particle before the n-th impact which occurs at $t = t_n$. If the particle crosses the barrier, then its velocity is not changed. Otherwise, it is reflected as if it had collided elastically with a rigid wall. In the reference frame of the moving barrier the particle's velocity before the impact is $V_n - v(t_n)$ and after the impact it becomes $-V_n + v(t_n)$. Therefore, in the rest reference frame the particle's new velocity is given by

$$V_{n+1} = -V_n + 2v(t_n). \tag{2.5}$$

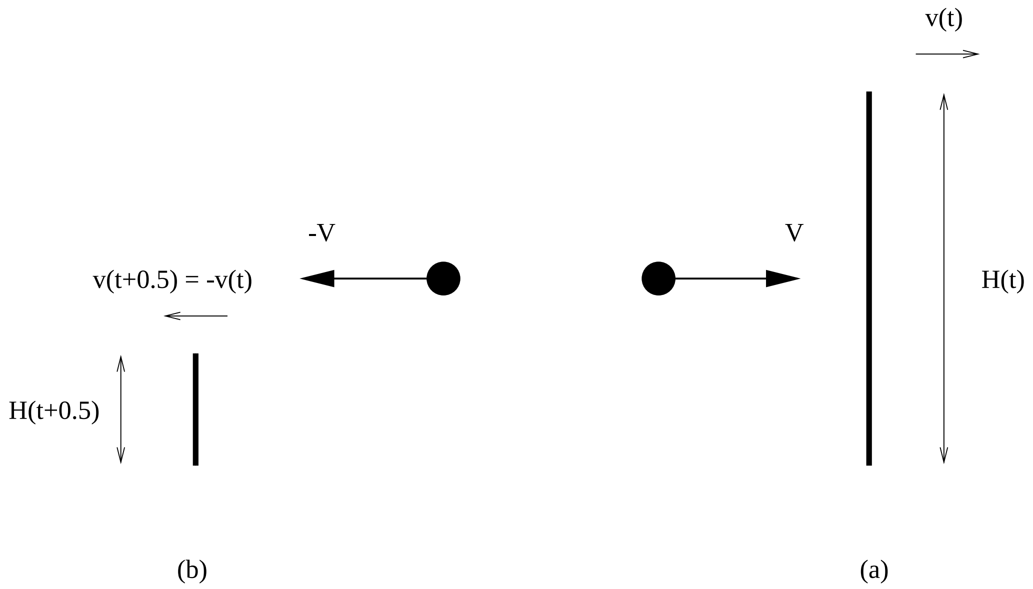

Figure 3: The symmetry breaking in the system. A particle having velocity V hits a barrier at t (a), and a particle having velocity $-V$ hits a barrier at $t + \frac{1}{2}$ (b). The relative speeds in both cases are the same, while the barriers' heights differ.

2.3 The Associated Mapping

The process described here is a deterministic one since V_{n+1} and t_{n+1} can, in principle, be calculated from V_n and t_n. In fact, we already explained how to calculate V_{n+1} in the previous section. Calculating t_{n+1}, the moment of the next collision is a much more difficult task. The difficulties originate from the fact that both the particle and the barriers move, and one has to find when they meet each other. An additional problem is the fact that a particle may collide a few times with the same barrier before moving to one of its neighbors. One has to decide whether the particle will re-collide with the same barrier or not. The equation for t_n is, thus, a rather complicated one, and in fact cannot be solved analytically for the sinusoidal wall velocity (Eq. (2.3)).

A simplification can be achieved in the following case. Let us assume that L, the distance between neighboring barriers is much larger than x_b, the amplitude of the barriers' motion. Suppose also that the velocity V of the particle is much larger than v_b, the maximal barriers' velocity. Since $V \gg v_b$, the particle performs only a single collision with the same barrier each time. We can assume that the distance which a particle travels between two consecutive collisions is exactly L. Since $L \gg x_b$, the calculated t_{n+1} would not be considerably modified by this approximation. Making this approximation, the "simplified" map can be easily written:

$$V_{n+1} = \begin{cases} V_n & \text{for } |V_n - v_b \sin(2\pi t_n)| > \sqrt{2H_0[1+\sin(2\pi t_n)]} \\ -\text{sign}(V_n)|V_n - 2v_b \sin(2\pi t_n)| & \text{for } |V_n - v_b \sin(2\pi t_n)| \leq \sqrt{2H_0[1+\sin(2\pi t_n)]}, \end{cases} \tag{2.6.a}$$

$$t_{n+1} = t_n + \frac{L}{|V_{n+1}|} \pmod 1. \tag{2.6.b}$$

Eq. (2.6.a) describes the two possible scenarios of crossing (the velocity is not changed) and reflection (the velocity is changed according to Eq. (2.5)). Note that for the case of reflection, Eq. (2.6.a) might differ from Eq. (2.5) in the narrow region of low velocities $|V| < 2v_b$. We use this slightly modified form, in which the velocity changes its sign after each reflection, in order to prohibit situations in which the particle collides with a barrier, changes its velocity but continues to propagate slowly in the <u>same</u> direction and re-collides with the same barrier. The assumption that the particle collides only once with a barrier is valid, however, only when $|V| \gg v_b$ and therefore, when $|V|$ is of the order of v_b, the simplified map becomes a bad approximation for the real dynamics. (The difficulties caused by this approximation are discussed later in this work.) Eq. (2.6.b) defines t_{n+1} under the assumption that the particle travels a distance L between two barriers.[3]

Throughout this work we set $L = 100$ ($L \gg x_b = \frac{1}{4\pi}$) in our numerical simulations. The amplitude of the barriers' velocity is $v_b = 2\pi x_b = \frac{1}{2}$, which means that the maximum change of velocity at an impact is $2v_b = 1$. The mean barrier's height, H_0, (which is also the amplitude of the change of the height) will serve as the control parameter in the problem. We shall examine how the nature of the dynamics changes with H_0.

[3]The "exact" problem, in which the actual motion of the barriers is considered, was treated in Refs. [13]–[15] for a piecewise linear wall velocity, and in Ref. [15] for a parabolic wall velocity. These references deal with the special case of the problem, called the Fermi accelerator, which is discussed in the next chapter.

3 The Fermi Accelerator

3.1 The Fermi Map

In 1949 Fermi [16] suggested an explanation for the mechanism of cosmic ray acceleration via collisions against moving irregularities of the interstellar magnetic field. He modeled this mechanism by considering the dynamics of a particle colliding with moving reflecting obstacles of very large mass. Ulam [17] introduced some simple problems involving the Fermi acceleration mechanism. The simplest problem is of a ball bouncing between two, infinitely heavy, oscillating walls. This problem is essentially the special case $H_0 = \infty$ of our problem, since the particle is trapped between two, infinitely high, barriers, being reflected from the one to the other. The map (2.6) for this special case reduces to:

$$V_{n+1} = -\mathrm{sign}(V_n) \cdot |V_n - 2v_b \sin(2\pi t_n)|, \tag{3.1.a}$$

$$t_{n+1} = t_n + \frac{L}{|V_{n+1}|} \pmod 1. \tag{3.1.b}$$

We shall describe now the features of the Fermi accelerator map by following the description of Lieberman and Lichtenberg ([13],[18]).[1] The Fermi map (3.1) is a special <u>symmetric</u> case of the problem to which we shall compare our results. While describing its features in the following sections, we introduce the "language" in use, dealing with dynamical maps. The terms introduced below, frequently appear in the discussion in any dynamical system.

3.2 Features of the Fermi Map

Fig. 4 shows a picture of the phase space $V - t$ of the map (3.1) which is a one-to-one transformation of this phase space into itself. We follow the trajectory $\{(V_n, t_n)\}$ of a particle, initially given low velocity V_0 and random phase t_0. While moving, the particle stochastically explores the available phase space and the picture of the phase space is

[1] References [13]–[15],[18] deal with a slightly different problem of a ball bouncing between a fixed and oscillating wall, i.e., only one of the walls imparts momentum to the particle. However, as appears from numerical simulations, this difference does not change significantly the features of the problem. Anyhow, comparing the results introduced here and in these references, one should consider this difference in the definitions of the problems.

constructed by plotting the trajectory's points. The motion within the available phase space is *ergodic* (see chapter 2 in Ref. [19] for definitions and basic properties of ergodic systems). This means that the same picture would arise if we had started at (almost) any other point in the available phase space Ω. The *equilibrium invariant distribution* is defined as the space probability, $P(\vec{x}) = P(V,t)$, which is:

1. Invariant with respect to the map $T(\vec{x})$, i.e.,

$$P(\vec{x})\|d\vec{x}\| = P(T(\vec{x}))\|T(d\vec{x})\|. \tag{3.2}$$

2. Having the space average over Ω equals to the time average of the motion:

$$\int_{\vec{x}\in\Omega} f(\vec{x})P(\vec{x})d(\vec{x}) = \lim_{N\to\infty}\frac{1}{N}\sum_{i=1}^{N} f(T^i(\vec{x}_0)) \tag{3.3}$$

(f is some observable function in Ω), for almost any $\vec{x}_0 \in \Omega$.

Numerically, $P(\vec{x})$ can be computed by allowing the trajectory to "wander through" Ω for many iterations and counting the number of times it passes through a small volume element surrounding $\vec{x}$. Denoting by $\Delta_{\vec{x}}$ the infinitesimal volume element containing $\vec{x}$, $P(\vec{x})$ is given by

$$P(\vec{x}) = \lim_{\Delta_{\vec{x}}\to 0}\lim_{N\to\infty}\frac{1}{N\Delta_{\vec{x}}}\sum_{i=1}^{N}\int_{\Delta_{\vec{x}}}\delta(T^i(\vec{x}_0)-\vec{z})d\vec{z}. \tag{3.4}$$

Eqs. (3.1) form an *area preserving map* which means that the area of a phase space element bounded by a closed curve is conserved under repeated iterations.[2] The general 2-dimensional map $T\begin{pmatrix} I_n \\ \theta_n \end{pmatrix} = \begin{pmatrix} I_{n+1} \\ \theta_{n+1} \end{pmatrix}$ is area preserving if $\mathbf{J}$, the Jacobian matrix of the map satisfies:

$$|\det(\mathbf{J})| = \left|\det\begin{pmatrix} \frac{\partial I_{n+1}}{\partial I_n} & \frac{\partial I_{n+1}}{\partial \theta_n} \\ \frac{\partial \theta_{n+1}}{\partial I_n} & \frac{\partial \theta_{n+1}}{\partial \theta_n} \end{pmatrix}\right| = 1. \tag{3.5}$$

[2]In general, *conservative systems* are those in which the volume of an element of the phase space is conserved in time, i.e., the flow in the phase space is incompressible. Hamiltonian systems are a class of conservative systems. The phase space coordinates are the canonical momenta p_i and coordinates q_i and the volume conservation property follows immediately from the Liouvile theorem:

$$\mathrm{div}\vec{j} = \sum_i\left(\frac{\partial \dot{p}_i}{\partial p_i} + \frac{\partial \dot{q}_i}{\partial q_i}\right) = \sum_i\left(\frac{\partial^2\mathcal{H}}{\partial p_i\partial q_i} - \frac{\partial^2\mathcal{H}}{\partial q_i\partial p_i}\right) = 0.$$

If the coordinates of the phase space are non-canonical then the measure is the conserved quantity.

The variables I and Θ are then said to be *canonical variables*.[3] The map (3.1) satisfies this condition and is therefore an area preserving one. Hence, we can set $\|d(\vec{x})\| = \|d(T(\vec{x}))\|$ in Eq. (3.2), which means that $P(\vec{x}) = P(T(\vec{x})) = \text{const}$. We thus conclude that the equilibrium invariant distribution is constant over the available phase space Ω.

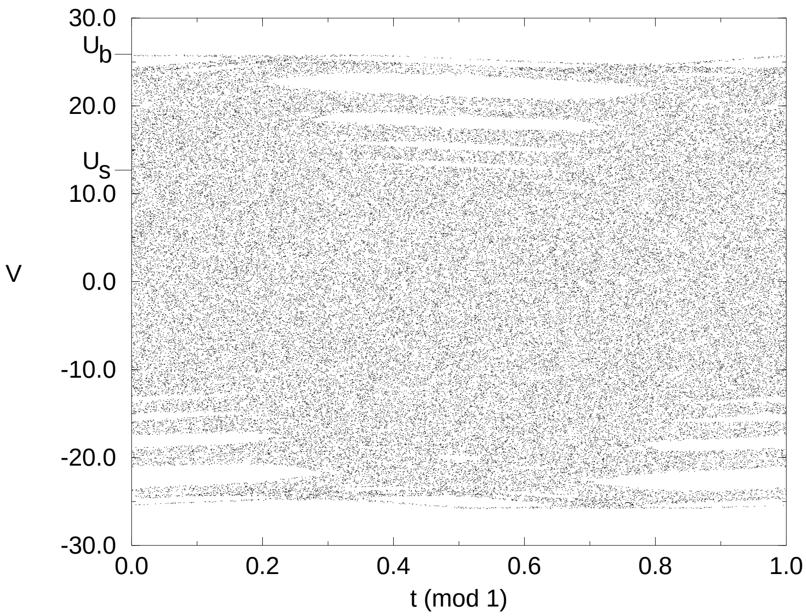

Figure 4: The available phase space Ω of the Fermi map (3.1) with $L = 100$ and $v_b = 0.5$. The picture was obtained by iterating the map $1.5 \cdot 10^7$ times and plotting the points $\{(V_n, t_n)\}$ of the trajectory. (Only every 199th iteration was plotted.)

In Fig. 4 we observe that the phase space Ω consists of three velocities regions:

1. The region of low velocities ($|V| < U_s$) in which the motion is stochastic over (almost) the entire region.

2. The region of intermediate velocities ($U_s < |V| < U_b$) in which the motion is stochastic only over part of the region. There exist some *islands*, embedded within the *stochastic sea*, which are inaccessible from outside. The motion in these islands (possible only if the trajectory was initially placed there) is regular (non stochastic) over elliptic-like curves (see next section).

[3]We use I and Θ as the canonical variables of the map to resemble action-angle variables, which are frequently chosen as a set of conjugate coordinates in the phase space of Hamiltonian systems. For Hamiltonian systems conjugate variables are also canonical (Liouvile Theorem). Here, I and Θ serve as a notation for canonical coordinates of the general 2-dimensional map and do not necessarily represent action-angle variables.

3. The region of high velocities ($|V| > U_b$). This region is inaccessible from below. The motion in this region (again, possible only if the trajectory was initially placed there) is mainly regular with only small isolated "bands" of stochastic motion.

We denote these regions by region (1), region (2) and region (3) respectively.

Fig. 5 shows the equilibrium invariant distribution integrated over time: $\tilde{P}(V) = \int_0^1 P(V,t)\,dt$. This quantity is the *probability density* of finding the particle with velocity V between two collisions. It was numerically computed by dividing the phase space into intervals of $\Delta V = 0.1$, iterating the map (3.1) $N = 2{\cdot}10^8$ times and counting the number of times the trajectory was found in each of the intervals. One can observe how $\tilde{P}(V)$ reflects the structure of the phase space. The uniform probability density at low $|V|$ represents region (1). The dips appearing at higher $|V|$ indicate the existence of inaccessible islands in region (2) (which clearly reduce the value of $\tilde{P}(V) = \int_0^1 P(V,t)\,dt$). In region (3), the probability density vanishes since the trajectory does not enter there. Notice that the picture shows $\tilde{P}(V)$ only for $V > 0$, however, from symmetry considerations (see section 3.4) the same picture is obtained for $V < 0$. Integrating $\tilde{P}(V)$, shown in Fig. 5, gives: $\int_0^\infty P(V)\,dV = \frac{1}{2}$.

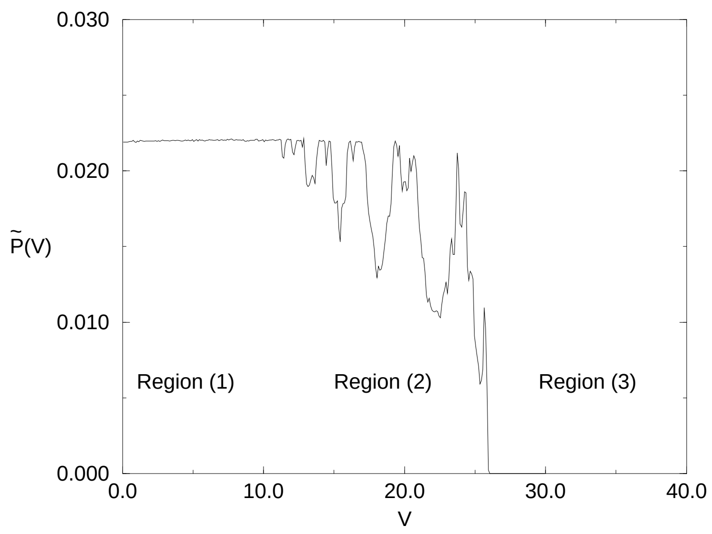

Figure 5: The probability density $\tilde{P}(V) = \int_0^1 P(V,t)\,dt$ of finding the particle with velocity $V > 0$, for the dynamics described by the the Fermi map (3.1) (with $L = 100$ and $v_b = 0.5$) . The phase space was divided into intervals of ΔV. Following a trajectory of $N = 2 \cdot 10^8$ iterations, the probability density was computed by counting the number of time the trajectory was found in each of the intervals. For $V < 0$, $\tilde{P}(V) = \tilde{P}(-V)$.

3.3 Regular Motion

What happens if we set the initial conditions of the particle's motion to lie in one of the inaccessible areas of Fig. 4 (the white areas inside the stochastic sea and the areas above or below it)? It appears that in this case, the character of the motion is very different from the stochastic "area-filling" motion in Ω. The motion takes place over some curves and is called "*regular*". Fig. 6 shows some regular curves and one stochastic trajectory of the Fermi map (3.1). (Since the velocity of the particle changes its sign every iteration, each trajectory is composed of two branches. The left and the right pictures show, respectively, the positive and the negative velocity branches of the curves.) Each of the curves, as well as the stochastic trajectory, originate from a different initial condition. The regular curves are of two types:

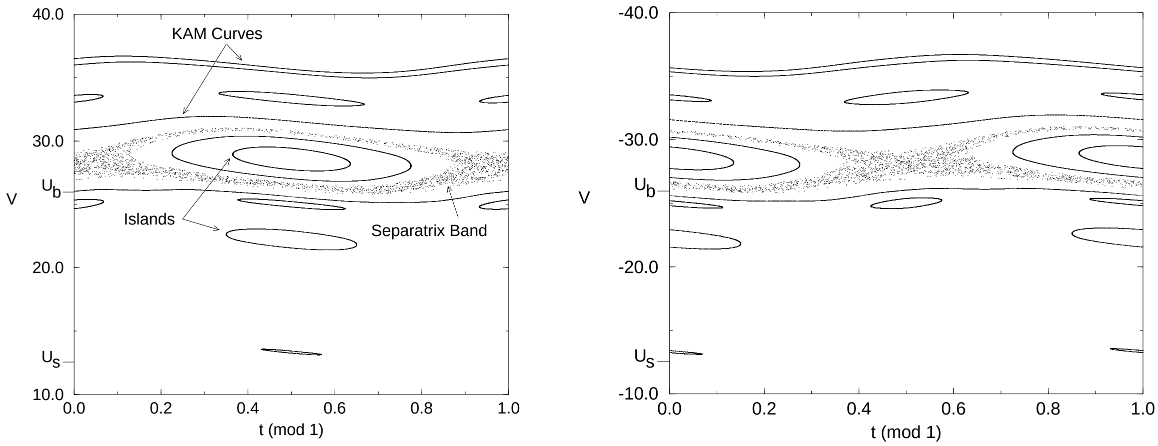

Figure 6: Some regular curves of the map (3.1) ($L = 100$ and $v_b = 0.5$). Each curve originates from a different initial condition. The curves are of two types: Elliptic orbits and KAM curves (see text below).The stochastic "band" is the separatrix band of the island. Since the velocity of the particle changes its sign every iteration, each trajectory is composed of two branches. The left and the right pictures show, respectively, the positive and the negative branches of the curves.

Elliptic orbits: An *elliptic* (stable) *periodic point* is located in the middle of each island. A periodic point of period n of the map T is a point which repeats itself, for the first time, after n applications of the map T, i.e., $T^n(\vec{x}_0) = \vec{x}_0$ and $T^i(\vec{x}_0) \neq \vec{x}_0$ for $i = 1, 2, \ldots, n-1$. The set of n different periodic points of period n $\{T^i(\vec{x}_0)\ ;\ i = 0, 1, \ldots, n-1\}$ is called a *cycle* of length n of the map T. If the particle is given initial condition which lies in the phase space close to one of the points of a (linearly) stable cycle, then the motion will be over n ellipses encircling the n periodic points of the cycle. The trajectory follows the cycle, but instead of jumping from a periodic point to another it moves from one ellipse to another. As the distance from the periodic point is increased, the motion remains regular over n closed curves, however, the shapes of the curves less and less resemble ellipses. Finally, at the edge of the island, a sudden change happens, and the motion becomes stochastic. In region (2) the last regular curve separates the island form the stochastic sea, thus defining its boundary. In region (3) the stochastic motion is over some narrow "bands", called *separatrix* bands, which are isolated by regular orbits. If the cycle is (linearly) unstable, then a trajectory, initially placed at the vicinity of one of the *hyperbolic* (unstable) periodic points of the cycle, would follow the cycle, but will gradually diverge from its points. In fact, at each separatrix band, surrounding a chain of n islands related to a stable n-cycle, there exists an unstable n-cycle. Each hyperbolic periodic point of this unstable cycle is located between two neighboring elliptic points of the stable cycle. If we start the motion in a separatrix band close to a hyperbolic point, $\vec{x}_0$, and follow the trajectory, we observe that after n iterations the trajectory returns to the vicinity of $\vec{x}_0$, but, it is found further from $\vec{x}_0$. It diverges from the hyperbolic point over a hyperbola and travels, in an irregular stochastic fashion, towards the neighboring hyperbolic point of the unstable cycle.

For the 2-dimensional area preserving map, it can be shown ([18], section 3.3b) that the cycle $\{T^i(\vec{x}_0)\ ;\ i = 0, 1, \ldots, (n-1)\}$ is linearly stable if and only if

$$|\mathrm{Tr}[\prod_{i=0}^{n-1} \mathbf{J}(T^i(\vec{x}_0))]| < 2, \tag{3.6}$$

where $\mathbf{J}(\vec{y})$ is the Jacobian matrix (see Eq. (3.5)) of the map T evaluated at $\vec{y}$. Looking at Fig. 4, one can see that the islands which occupy the largest areas in region (2) are those related to 2-cycles of the form $\vec{x}_0 = (V = +\frac{2L}{2n+1}, t = \frac{1}{2})\ ;\ \vec{x}_1 = (V = -\frac{2L}{2n+1}, t = 0)$, where n is an integer. Using the condition of linear stability (3.6), one can find that the cycles $\{\vec{x}_0, \vec{x}_1\}$ are stable for $|V| > \sqrt{\frac{\pi L}{2}}$. The "inverse" cycles $\vec{x}_0 = (V = -\frac{2L}{2n+1}, t = \frac{1}{2})\ ;\ \vec{x}_1 = (V = +\frac{2L}{2n+1}, t = 0)$ are unstable for all values of V. Therefore, no islands appear around the points of these cycles which are hidden in the stochastic sea. Other islands, at region (2), seen to the naked eye, are those related to the stable cycles of the form $\vec{x}_0 = (V = +\frac{L}{n}, t = 0)\ ;\ \vec{x}_1 = (V = -\frac{L}{n}, t = 0)$ and $\vec{x}_0 = (V = +\frac{L}{n}, t = \frac{1}{2})\ ;\ \vec{x}_1 = (V = -\frac{L}{n}, t = \frac{1}{2})$. These islands are stable for $|V| > \sqrt{\pi L}$.

For larger cycles of length $2k$ (cycles of the map (3.1) must be of even length), questions of existence and stability are more complicated. However, Lieberman and Lichtenberg [13] noted that the larger the value of k, the larger the value of the associated $|V|$ below which $2k$-cycles become unstable. Cycles of length 2 are the last to lose their stability when $|V|$ is decreased. One can expect that the value $|V| = U_s = \sqrt{\frac{\pi L}{2}}$, related to the loss of stability of the 2-cycles mentioned above, is the lower bound for the existence of any stable cycle and surrounding islands. This, however, turns to be inaccurate. A careful look at Fig. 5 reveals the existence of two small dips, indicating the existence of inaccessible islands, at the velocity range 11–12, i.e., lower than $U_s = \sqrt{\frac{100\pi}{2}} \approx 12.5$. The islands, related to these dips, are not seen while looking at Fig. 4 and we are not able to point out which are their corresponding cycles. Anyhow, one can always derive U_s from $\tilde{P}(V)$, in a more precise way than looking at the phase space plot.

KAM curves: The KAM curves (named after Kolmogorov, Arnold and Moser [20]–[24]) are the wiggly horizontal lines which appear in Fig. 6, stretched from one end of the picture to the other. The phase space is divided by these curves into a set of bounded areas which are mutually inaccessible. In order to understand the appearance of these curves we should briefly review the KAM theorem . (For a detailed summary of the KAM theorem see [18], section 3.2.)

A system is called *integrable* if one can find a set of variables $\vec{I}, \vec{\Theta}$ such that in this coordinate system the motion is regular over the curves (*tori*) $\vec{I} = \vec{I}_0$. If the equations of motion are similar to those of an integrable system with some additional small perturbation terms, then the system is said to be nearly integrable. The KAM theorem states that for a sufficiently small perturbation and sufficiently a smooth one (i.e., the function describing the perturbation has a sufficient number of continuous derivatives), some of the regular tori still exist, although suffer a small modification. As the perturbation is increased, the distortion of the regular tori is increased and less of them survive, until at some perturbation strength they all disappear. For 2-dimensional (area) mappings, KAM curves create isolated regions of the phase space and prevent the trajectories from leaving these regions. At higher dimensions, there is the so called *Arnold Diffusion* which allows the access of a trajectory to the entire phase space. For the Fermi map (3.1) the first KAM curve, at $|V| \approx U_b$, bounds the stochastic sea from above, thus preventing a particle, initially placed below, from being accelerated to higher velocities. Moreover, at region (3), stochastic motion exists only over some narrow bands since these bands are bounded form above and below by KAM curves.

The existence of KAM curves for $|V| > U_b$ is in agreement with the KAM theorem. In order to understand this we should notice that for $v_b = 0$ the map (3.1) describes an integrable motion on the set of tori $|V| = V_0$. For $v_b \neq 0$ we locally approximate the map (3.1) in a region close to some $|V| = V_0$. Taking V_0 to satisfy $L/V_0 = m$ (m integer), the local (linearized) map is:

$$I_{n+1} = I_n + K \sin \Phi_n, \tag{3.7.a}$$

$$\Phi_{n+1} = \Phi_n + I_{n+1}, \tag{3.7.b}$$

where $K = 4\pi v_b L/V_0^2$, $I_n = -2\pi L \Delta V_n / V_0^2$ and $\Delta V_n = |V_n| - V_0$. The map (3.7) is the *standard mapping* (also known as the Chirikov-Taylor mapping). The *stochasticity parameter*, K, measures the deviation of the map from integrability. For K smaller than some value, i.e., V_0 larger than some value, we expect the existence of KAM curves, which will be the perturbed tori $|V| = \text{const}$. Numerical and analytical studies (see [18], chapter 4, for details) of the standard mapping demonstrated that for $K \lesssim 0.97$, KAM curves exist. For the linearized Fermi accelerator map, $K = 4\pi v_b L/V_0^2$. This means the largest V_0 in the set $\{V_0 = \frac{L}{m}, m\text{-integer}\}$ that lies in the stochastic sea is (for $L = 100$ and $v_b = 0.5$) $V_0 = 25$, which corresponds to $K \approx 1$. It is indeed in agreement with Fig. 4.

3.4 Symmetry

From Figs. 4 and 6, one can see that the picture of the upper half of the phase space ($V > 0$) is different from the picture of the lower half ($V < 0$). However, cutting the picture of the lower half of the phase space along the $t = \frac{1}{2}$ axis and joining the two pieces along the $t = 0$ axis instead, yields the same picture as that of the upper half (see Fig. 7). This property is due to the fact that the velocity of the walls at any given time, t, is the negative of its value for $t - \frac{1}{2}$. As stated above (Section 2.2), this "inverse" symmetry is broken in the problem represented by the map (2.6) , due to the difference in the height of the barriers at t and $t - \frac{1}{2}$.

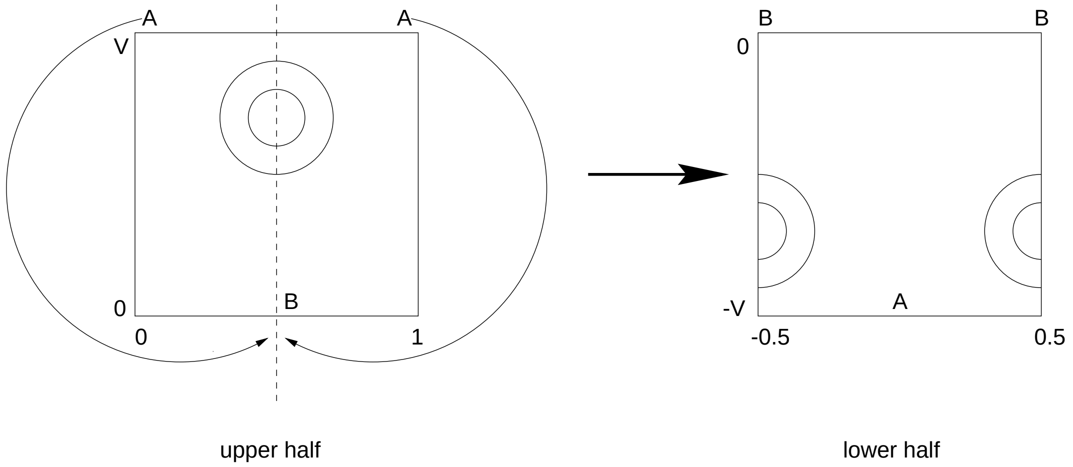

Figure 7: The "inverse" symmetry between the upper and the lower halves of Ω, the phase space of the Fermi map. Cutting the upper half along the $t = \frac{1}{2}$ axis and joining the two pieces along the $t = 0$ axis (in a way that the two points A are joined together), yield the picture of the lower half.

4 General Properties of the System

4.1 Asymmetry Parameters

We now turn to investigate the map (2.6) for finite potential heights H_0. As in the Fermi accelerator problem, we let a particle, initially given low velocity and random phase, explore the available phase space Ω_{H_0}.[1] Numerical simulations show that the resulting phase space plot is independent of initial conditions (provided the initial velocity is sufficiently low), which implies that the motion in Ω_{H_0} is ergodic.[2]

We follow the stochastic motion of a particle in a potential field composed of a set of equally spaced potential barriers, where the m-th barrier is oscillating around the point $x = mL$ (L is the spacing between neighboring barriers). The motion of the particle, described by the map (2.6), is asymmetric and can be characterized by the mean displacement of the particle and the related drift velocity. Suppose that at time t_0 a particle with velocity V_0 hits the barrier located near $x = 0$. Then, it goes through a set of n collisions with the barriers and at a time t_n it hits the m-th barrier, where $m = m(V_0, t_0, n)$ is a function of initial conditions and the number of iterations. Let $\{V_1, \ldots, V_n\}$ be the set of velocity values that the particle had from $t = t_0+$ until $t = t_n$. We denote by n_1 and n_2 the numbers of positive and negative values among them respectively, where positive (negative) velocity indicates a motion to the right (left). One can easily verify that the position of the particle at $t = t_n$ satisfies $x(V_0, t_0, n) = x_n = mL = (n_1 - n_2)L$. The mean displacement per collision of the particle, $\langle d \rangle$, is defined as:

$$\langle d(V_0, t_0) \rangle = \lim_{n\to\infty} d_n = \lim_{n\to\infty} \frac{1}{n} x_n = \lim_{n\to\infty} \frac{1}{n}(n_1 - n_2)L. \tag{4.1}$$

This, however, is the time average of the function

$$h(V, t) = \begin{cases} +1 & V > 0 \\ -1 & V < 0 \end{cases} .$$

[1] The available phase space of the map (2.6) will be denoted by Ω_{H_0}, while for the special case of the Fermi accelerator problem we use the notation Ω.

[2] A dynamical system is ergodic if, and only if, it is *indecomposable*, i.e., if there does not exist any invariant set of non vanishing measure in the phase space, except for the whole phase space itself. The fact that the same picture of phase space is obtained by plotting trajectories initially starting at different points, suggests that the system is indecomposable and that the obtained plot shows the whole available phase space. However, using numerical simulations to determine whether a system is ergodic or not, raises questions concerning the numerical process and its limitations. We refer the reader to Appendix A where we discuss these questions.

From the fact that the system is ergodic, we deduce that:
a. $\langle d(V_0, t_0)\rangle$ exists and is independent of initial conditions for all (V_0, t_0) in Ω_{H_0}.
b. The time average in the definition of $\langle d\rangle$ can be replaced by a space average of the function $h(V,t)$ over Ω_{H_0}. We can thus write

$$\frac{\langle d(V_0, t_0)\rangle}{L} = \iint_{(V,t)\in\Omega_{H_0}} h(V,t)P(V,t)\, dV\, dt = \int_{V>0} \tilde{P}(V)\, dV - \int_{V<0} \tilde{P}(V)\, dV = \frac{\langle d\rangle}{L}, \tag{4.2}$$

where $P(V,t)$ is the equilibrium invariant distribution (see Eqs. (3.2)–(3.4)), and $\tilde{P}(V)$ is the probability density of finding the particle with velocity V between two collisions: $\tilde{P}(V) = \int_0^1 P(V,t)\, dt$. The average time interval between two consecutive collisions is given by:

$$\langle \Delta t\rangle = \int \frac{L}{|V|}\tilde{P}(V)dV, \tag{4.3}$$

and the average drift velocity of the particle is:

$$V_{\rm drift} = \frac{\langle d\rangle}{\langle \Delta t\rangle}. \tag{4.4}$$

From Eqs. (4.2)–(4.4) we see that the knowledge of $\tilde{P}(V)$ allows us to calculate the quantities we are interested at. For the Fermi accelerator problem $\tilde{P}(V) = \tilde{P}(-V)$, which immediately yields: $\langle d\rangle = V_{\rm drift} = 0$. It will be shown that for finite H_0 this symmetry is broken.

4.2 Features of the Map

The Fermi map (3.1), which is the special case $H_0 = \infty$ of the map (2.6), is a one-to-one area preserving transformation of Ω, the available phase space, onto itself. We now show that these properties hold for any finite H_0.

Theorem 1 *The map (2.6) is a one-to-one transformation of Ω_{H_0} onto itself.*

Proof:

Let T_{H_0} denote the map (2.6) for some finite H_0, $T_{H_0} : \Omega_{H_0} \longrightarrow \Omega_{H_0}$. By definition, any point in Ω_{H_0} has at least one source there. To show that it has exactly one source, we divide

Ω_{H_0} into two subsets: $A_{\rm cross}$, the set of points (V,t) in Ω_{H_0} that satisfy $|V-v(t)| > \sqrt{2H(t)}$, and $A_{\rm ref}$, the set of points (V,t) in Ω_{H_0} satisfying $|V-v(t)| \leq \sqrt{2H(t)}$. (If a particle with velocity V hits a barrier at time t and crosses it then $(V,t) \in A_{\rm cross}$, while if it is reflected from the barrier then $(V,t) \in A_{\rm ref}$.) The points in each subset are mapped in different ways (by different "sub-maps", see Eq. (2.6.a)). Assuming that $V > 2v_b$, one can easily see that two points of the same subset cannot be mapped into the same point. Therefore, we just have to show that a point cannot have two sources, one in $A_{\rm cross}$ and one in $A_{\rm ref}$. This can be easily shown: Let (V^*,t^*) be a point in Ω_{H_0}. If the source of this point lies in $A_{\rm cross}$, then it is the point $(V^*, t^*-\frac{L}{|V^*|})$, and it satisfies $|V^*-v(t^*-\frac{L}{|V^*|})| > \sqrt{2H(t^*-\frac{L}{|V^*|})}$. On the other hand, if the source of the point (V^*,t^*) lies in $A_{\rm ref}$, then it is the point $(-V^*+2v(t^*-\frac{L}{|V^*|}), t^*-\frac{L}{|V^*|})$ and it satisfies $|-V^*+2v(t^*-\frac{L}{|V^*|})-v(t^*-\frac{L}{|V^*|})| = |V^*-v(t^*-\frac{L}{|V^*|})| \leq \sqrt{2H(t^*-\frac{L}{|V^*|})}$. These two cannot, of course, be satisfied simultaneously, and we have thus completed the proof.

Theorem 2 *The map (2.6) is area preserving.*

Proof:

We want to show that $\|d\vec{x}\| = \|T_{H_0}(d\vec{x})\|$ for every $\vec{x}$ in Ω_{H_0}. The points in the area element $d\vec{x}$ can be divided between the two subsets $A_{\rm cross}$ and $A_{\rm ref}$. Hence, we can write $d\vec{x} = d\vec{x}_1 \cup d\vec{x}_2$, where $d\vec{x}_1$ and $d\vec{x}_2$ are included in $A_{\rm cross}$ and $A_{\rm ref}$ respectively, which means $d\vec{x}_1 \cap d\vec{x}_2 = \{\emptyset\}$. It can be easily shown, using the condition (3.5), that each sub-map of the map (2.6) is area preserving, i.e., $\|d\vec{x}_1\| = \|T_{H_0}(d\vec{x}_1)\|$ and $\|d\vec{x}_2\| = \|T_{H_0}(d\vec{x}_2)\|$. Using this, and the fact that T_{H_0} is a one to one map (Theorem 1), which implies $T_{H_0}(d\vec{x}_1) \cap T_{H_0}(d\vec{x}_2) = \{\emptyset\}$, we can write the set of equalities:

$$\begin{aligned}\|d\vec{x}\| &= \|d\vec{x}_1\| + \|d\vec{x}_2\| = \|T_{H_0}(d\vec{x}_1)\| + \|T_{H_0}(d\vec{x}_2)\| \\ &= \|T_{H_0}(d\vec{x}_1 \cup d\vec{x}_2)\| = \|T_{H_0}(d\vec{x})\|. \qquad \text{(Q.E.D.)}\end{aligned} \tag{4.5}$$

Corollary *The equilibrium invariant distribution $P(V,t)$ is constant over Ω_{H_0}.*
Proof: This immediately follows form Eq. (3.2) and Theorem 2 (Eq. (4.5)).

So far we have seen the similarities between Fermi map (3.1) and the map (2.6), for a finite H_0. Both maps, applied on initial conditions of low velocity and random phase, describe a stochastic motion over the available phase space Ω_{H_0} (or Ω, in the Fermi accelerator problem). This motion, in both cases, is ergodic with a constant equilibrium invariant distribution. Since the equilibrium invariant distribution is constant over Ω_{H_0},

$\tilde{P}(V) = \int_0^1 P(V,t)\,dt$, the probability density of finding the particle with velocity V between two collisions, can be derived from the knowledge of the structure of Ω_{H_0}. The remainder of the work will be devoted to the investigation of Ω_{H_0}.

One of the major differences between Ω_{H_0} and Ω, is the KAM boundary which bounds Ω from above and does not appear in Ω_{H_0} for finite H_0. This difference can be understood if we remember that one of the requirements of the KAM theorem for the existence of KAM curves, is sufficient smoothness of the perturbation (See section 3.3).[3] This is not the case when H_0 is finite. Fig. 8 shows how the $(V-t)$ space is divided between the sets A_{cross} and A_{ref}, which are mapped by the two sub-maps of crossing and reflection, respectively. The two (for positive and negative V) curves $|V - v(t)| = \sqrt{2H(t)}$, separate between the different regions and the map (2.6) is discontinuous over these curves. The requirements of the KAM theorem are thus not fulfilled, and therefore no KAM curve bounds Ω_{H_0}.

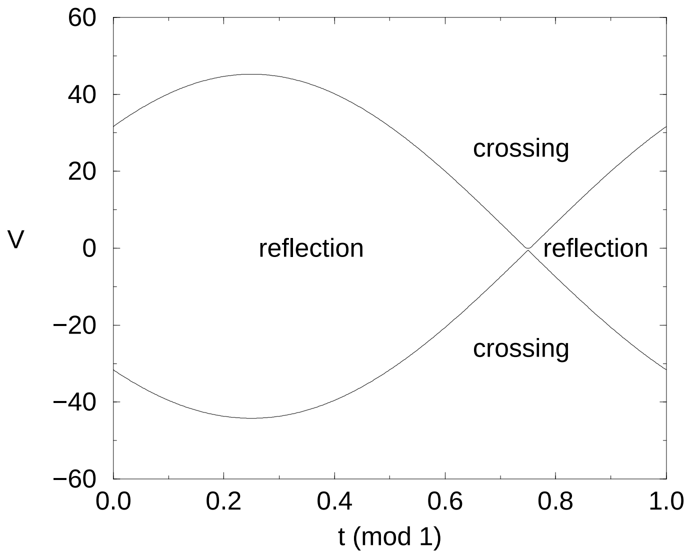

Figure 8: Regions in the $(V-t)$ space of points mapped by the sub-maps of crossing and reflection respectively, for the case of $H_0 = 500$. The map T_{H_0} is discontinuous over the curves separating between the different regions.

The KAM boundary in Ω defines a speed bound since the trajectory in the phase space cannot cross it and move to a region of higher speeds. In Ω_{H_0}, this type of speed

[3]For 2-dimensional (area) map, two continuous derivatives would be sufficient for the existence of KAM curves (depending of course also on the the strength of the perturbation) and one continuous derivative is a necessary condition.

barrier does not exist, however, other reasons lead to the appearance of different velocity bounds. In Fig. 8 we see that for $V > V_{\max}$ and $V < V_{\min}$, all points in $(V-t)$ space lie in $A_{\rm cross}$. For these velocity values, the map (2.6) is reduced to

$$V_{n+1} = V_n, \tag{4.6.a}$$

$$t_{n+1} = t_n + \frac{L}{|V_{n+1}|}. \tag{4.6.b}$$

This map however describes an integrable system (see section 3.3 for definition) in which the motion is over the tori $V = $ const. If the velocity of the particle is larger than $V_{\max}$ or smaller than $V_{\min}$, then it will always cross the barriers, regardless the moment of impact. Its velocity, clearly, will never change.

The $(V-t)$ space is thus composed of the region $V_{\min} < V < V_{\max}$, where the motion is stochastic (which might however include some inaccessible islands of regular motion), and the regions $V < V_{\min}$ and $V > V_{\max}$ in which the motion is regular over the tori $V = $ const. For finite H_0, it is therefore the tori $V = V_{\min}$ and $V = V_{\max}$ which serve as the velocity barriers of the phase space. These bounds can be computed by considering the collision of a particle with a barrier at $t = \frac{1}{4}$, when the hight of the barrier is the largest (see Fig. 8). In order for a particle to collide with a barrier at $t = \frac{1}{4}$ and still be reflected it should satisfy $|V - v_b| \leq 2\sqrt{H_0}$, which means that:

$$V_{\max} = 2\sqrt{H_0} + v_b, \tag{4.7.a}$$

and

$$V_{\min} = -(2\sqrt{H_0} - v_b). \tag{4.7.b}$$

The fact that the values $V_{\min}$ and $V_{\max}$ are the extremal velocities which a particle may gain, can be shown explicitly:

Theorem 3 *If* $V_{\min} < V_n < V_{\max}$, *then also,* $V_{\min} < V_{n+1} < V_{\max}$

Proof:

If the moment of impact, t_n, was such that the particle crossed the barrier, then $V_{n+1} = V_n$ and, of course, $V_{\min} < V_{n+1} < V_{\max}$. If the particle is reflected from the barrier, then $V_{n+1} = -V_n + 2v(t_n)$. Since the particle was reflected from the barrier, it is obvious that $|V_n - v(t_n)| \leq \sqrt{2H(t_n)}$. This can be also written in the following way: $|-V_n + 2v(t_n) - v(t_n)| = |V_{n+1} - v(t_n)| \leq \sqrt{2H(t_n)}$, which implies that $(V_{n+1}, t_n) \in A_{\rm ref}$.

This, however, means that the particle did not move into the region of regular motion, $V > V_{\max}$ or $V < V_{\min}$, in which $(V,t) \in A_{\rm cross}$ for all values of t. We have thus proved that even if the particle was reflected from a barrier at the n-th collision, still, $V_{\min} < V_{n+1} < V_{\max}$.

4.3 Random Phase Approximation

In the previous section we have shown that a particle with initial velocity between $V_{\min}$ and $V_{\max}$, will stay within these bounds forever. The simplest assumption is that the whole space between these two bounds is included in the phase space. Given that the velocity of the particle satisfies $V_{\min} < V_n < V_{\max}$, we assume that it can collide with a barrier at any time (phase). This assumption prohibits the existence of any inaccessible islands. Further assuming that the distribution is constant over this phase space, we conclude that

$$\tilde{P}_{\rm RPA}(V) = \begin{cases} \frac{1}{|V_{\max}-V_{\min}|} = \frac{1}{4\sqrt{H_0}} & V_{\min} < V < V_{\max} \\ 0 & \text{otherwise} \end{cases}, \tag{4.8}$$

where $V_{\min}$ and $V_{\max}$ are given by Eqs. (4.6) . Using this in Eq. (4.2) and Eq. (4.3), we find that

$$\langle d \rangle_{\rm RPA} = \frac{v_b L}{2\sqrt{H_0}}, \tag{4.9}$$

and

$$\langle \Delta t \rangle_{\rm RPA} = \frac{L}{4\sqrt{H_0}} \int_{V_{\min}}^{V_{\max}} \frac{dV}{|V|}. \tag{4.10}$$

Two remarks should be made:

1. This approximation is called the random phase approximation (RPA), since the same results are obtained if we replace the process which determines the phase [Eq. (2.6.b)], by the assumption that the phase is a random variable (with a uniform probability density). Making this assumption immediately yields that $P_{\rm RPA}(V,t)$ is independent of t. One can write then a Fokker-Planck equation describing the evolution of $\tilde{P}_{\rm RPA}(V)$ in time.[4] The boundary conditions require that the probability currents at $V = V_{\min}$ and $V = V_{\max}$ vanish. The steady state solution of the equation is the probability density

[4] Actually, it is more convenient to define $P_1(V)$ for $V > 0$ and $P_2(V)$ for $V < 0$ and write a set of two coupled Fokker-Planck equations.

$\tilde{P}_{\rm RPA}(V)$. It can be numerically computed using a Monte-Carlo technique, by iterating Eq. (2.6.a) and using some random-numbers generator to produce the set of $\{t_n\}$. Using a large number of iterations, the probability density, $\tilde{P}_{\rm RPA}(V)$, is computed by dividing the phase space into small velocity intervals ΔV, and counting the number of times the velocity is found in each of these intervals. We performed this procedure for various values of H_0, and obtained a constant equilibrium probability density for all of them (see Fig. 9).

2. The integral in Eq. (4.10) diverges since the point $V = 0$ is included in the range of integration and $\tilde{P}(0) \neq 0$. Consequently, the drift velocity vanishes, $V_{\rm drift} = 0$ (Eq. (4.4)). This, however, does not mean that the system is symmetric since $\langle d \rangle_{\rm RPA} \neq 0$. The origin of this behavior is the fact that the map is simplified and does not describe the dynamics properly when the velocity of the particle V is of the order of v_b (the characteristic velocity of the barriers) or less (see section 2.3).[5] In Appendix B we explain why dealing with an "exact" problem, one should find that $\tilde{P}(0) = 0$, and show how $\langle d \rangle$ and $V_{\rm drift}$ depend on H_0 and v_b.

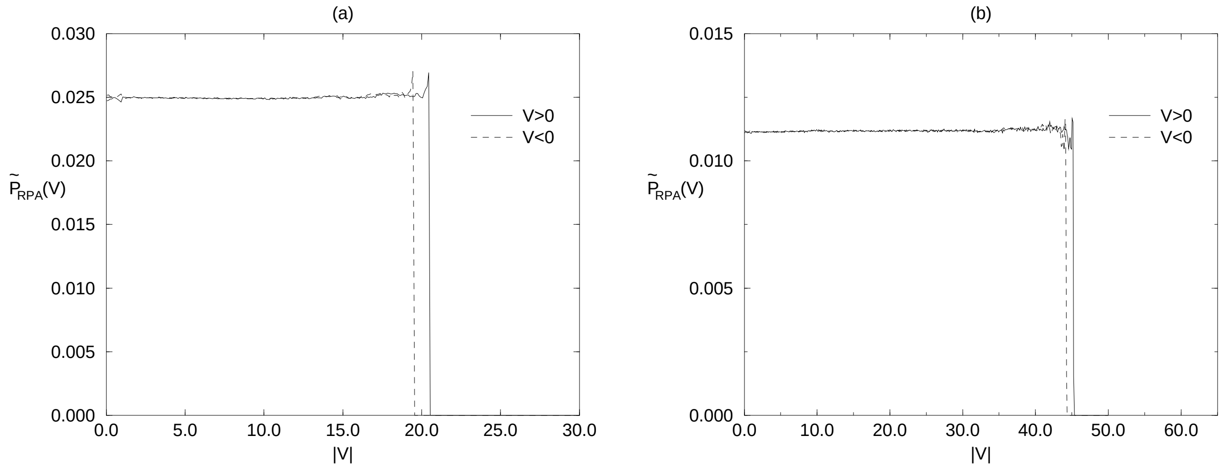

Figure 9: $\tilde{P}_{\rm RPA}(V)$ computed for (a) $H_0 = 100$ and (b) $H_0 = 500$ ($v_b = 0.5$). Collisions times $\{t_n\}$ were chosen randomly with a uniform probability density over the interval $[0, 1)$, while Eq. (2.6.a) was iterated for $N = 5 \cdot 10^8$ times. The solutions were computed by dividing the phase space into small velocity intervals $\Delta V = 0.1$ and counting the number of times the velocity was found in each of these intervals.

To summarize, making the random phase approximation, the resulting dynamics are characterized by two main features:

1. The net motion is directed from left to right ($\langle d \rangle_{\rm RPA} > 0$) for all values of H_0.
2. The mean displacement per collision, $\langle d \rangle_{\rm RPA}$, is a continuous function of H_0 (decreasing

[5]The same behavior is found when dealing with the simplified Fermi map (see Fig. 5)

as $1/\sqrt{H_0}$). It is also reasonable to assume that $V_{\rm drift}$, obtained after a proper correction of $\tilde{P}(V)$ at the low velocities, is a continuous function of H_0. In Appendix B we show that for the exact problem we find that $V_{\rm drift}$ decreases approximately as $(\ln H_0)^{-1}$.

The RPA assumption holds in a system where the spacings between neighboring barriers are random. In our system there is a constant distance between the barriers and therefore phase correlations appear and modify the RPA results. This subject is discussed in the next chapter.

5 Numerical Results

5.1 Low Barrier Heights

We now introduce some of the results obtained by iterating the map (2.6) for various values of H_0. We start with low values of the control parameter ("low" will be defined in the next section). Fig. 10 shows plots of the phase space, Ω_{H_0}, together with the corresponding probability densities, $\tilde{P}(V)$. One can clearly see that the obtained results are similar to those derived using random phase approximation (RPA) in section 4.3. The available phase space includes the entire velocity region $V_{\min} < V < V_{\max}$ where no embedded islands appear at all. Since we already know that $P(V,t)$ is constant, this immediately implies that $\tilde{P}(V) = \tilde{P}_{\mathrm{RPA}}(V) = \text{const.}$ (Eq. (4.8)), which in turn implies that $\langle d \rangle = \langle d \rangle_{\mathrm{RPA}}$ (Eq. (4.9)).

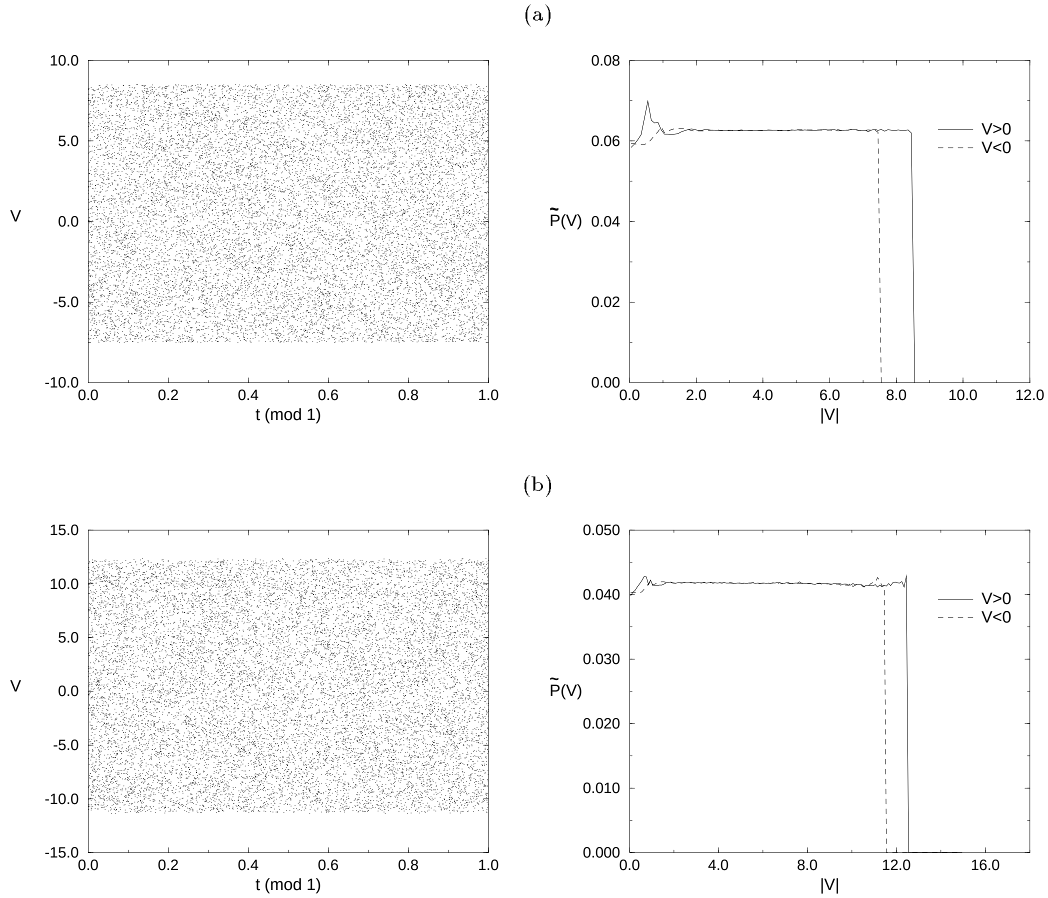

Figure 10: The available phase space, Ω_{H_0}, (left) and the probability density, $\tilde{P}(V)$, (right) for (a) $H_0 = 16$ and (b) $H_0 = 36$ ($L = 100$ and $v_b = 0.5$). The small deviations from the constant value at low velocities are probably due to the fact that the map (2.6) is not a one-to-one transformation for $|V| < 2v_b$.

The fact that RPA correctly describes the dynamics when H_0 is small, is actually not surprising. The velocity of the particle is bounded between $V_{\min}$ and $V_{\max}$, which increase proportionally to $\sqrt{H_0}$ (see Eqs. (4.6)). For low speeds the time interval between two consecutive collisions, $L/|V|$, is at least a few times larger than the period of the barriers' motion, τ, thus leading to weak correlations between consecutive phases. This seems to explain why embedded islands, which indicate strong phase correlations, do not appear at low speeds. It will be shown in the next section that for larger H_0, islands begin to appear since higher speeds are included in the phase space, Ω_{H_0}. Yet, as in the case of the Fermi map (chapter 3), there is a threshold speed $U_s(H_0)$, below which islands do not appear.[1] Anyhow, the set of phases $\{t_n\}$ looks as if it is a random sequence of numbers uniformly distributed over $[0, 1)$. Since, the results obtained by iterating the map are the same as those obtained by assuming the phase is a random variable, then, at least for this purpose, we can regard the deterministic process which generates the set $\{t_n\}$ as a "random numbers generator".[2]

5.2 Phase Correlations

5.2.1 Embedded Islands

Increase of H_0 leads to the inclusion of higher speeds in Ω_{H_0} and the appearance of embedded islands above the threshold speed $U_s(H_0)$. The phenomenon emerges when H_0 exceeds the value of 40–50 (assuming, as usual in this work, that $L = 100$ and $v_b = 0.5$). Figs. 11.a–c show plots of Ω_{H_0} for some values of H_0, together with the corresponding probability densities, $\tilde{P}(V)$.

[1]The quantity U_s is used in this work (chapter 3) and in other references (Refs. [13],[18]) to denote $U_s(H_0)$ for the special case of the Fermi map (3.1). However, when H_0 is sufficiently large, many of the islands that appear in Ω, the available phase space of the Fermi map, also appear in Ω_{H_0}. In particular, this is true for the large 2-cycle islands of Ω (see section 3.3). This happens since for large H_0 these islands are completely located in A_{ref}, the part of Ω_{H_0} which is iterated by the sub-map of reflection, and the sub-map of reflection is actually the Fermi map.

[2]Random numbers generators are deterministic algorithms used to produce sequences of numbers which *appear* to be random. The numbers are not really random of course since each number in the sequence depends on the preceding one. The concept of randomness can be mathematically formulated in several ways and there are many possible tests for its detection (or more correctly, for the detection of non-randomness). The reader can find extended discussions (using different approaches) of this issue in Ref. [25], chapter 3 and in Ref. [26], chapter 10.

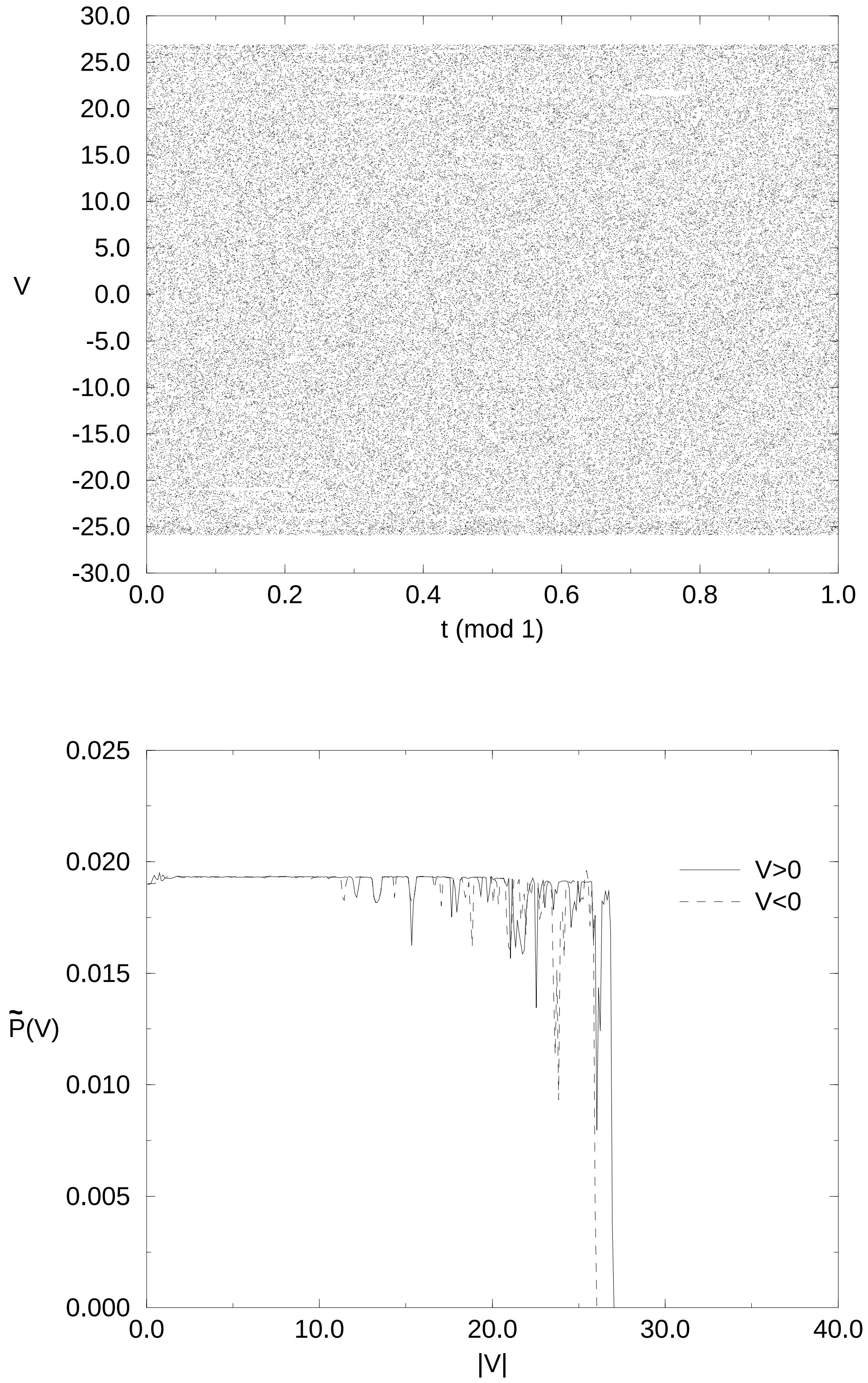

Figure 11.a: The available phase space Ω_{H_0} (top) and the corresponding probability density $\tilde{P}(V)$ (bottom) for $H_0 = 175$.

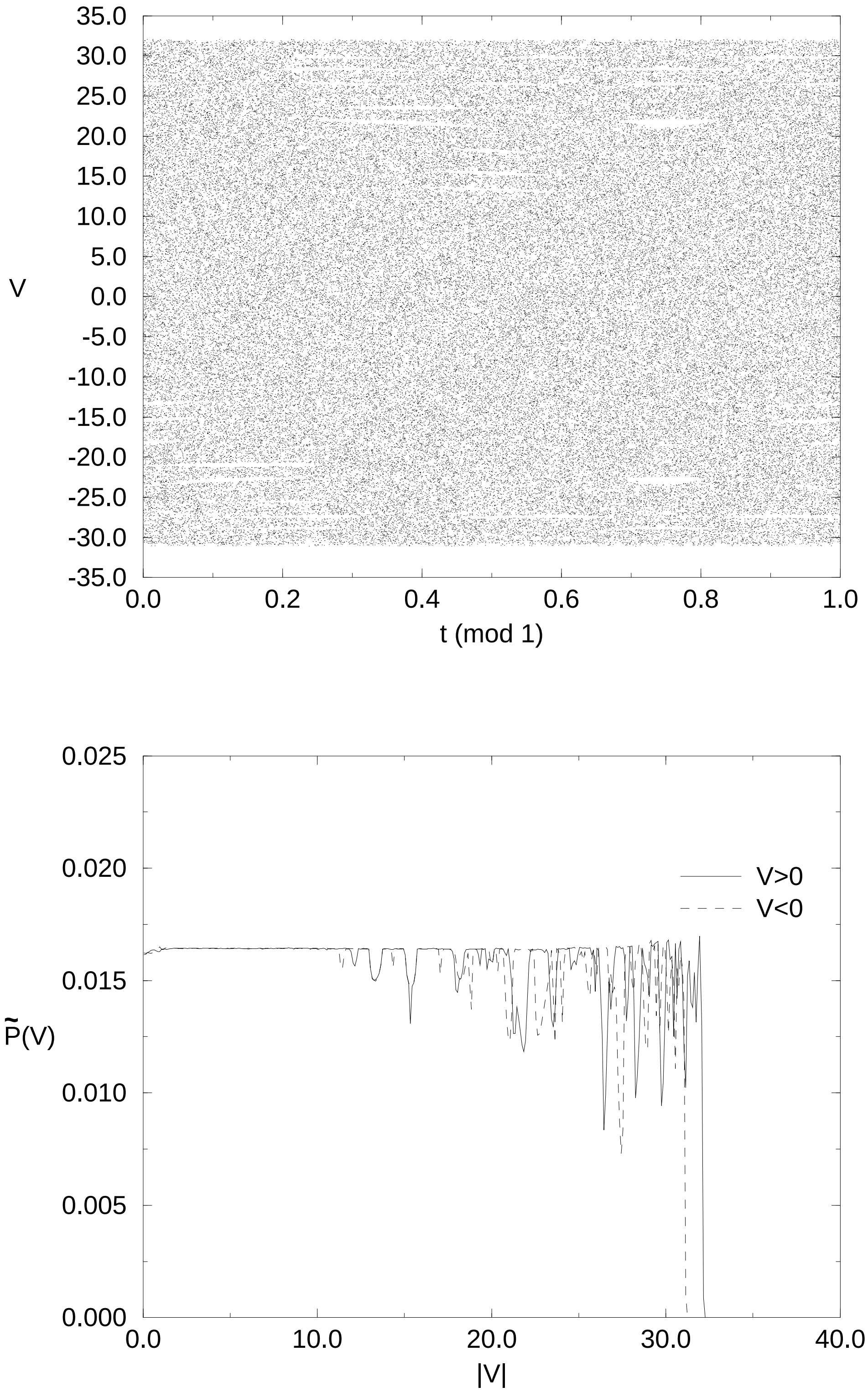

Figure 11.b: The available phase space Ω_{H_0} (top) and the corresponding probability density $\tilde{P}(V)$ (bottom) for $H_0 = 250$.

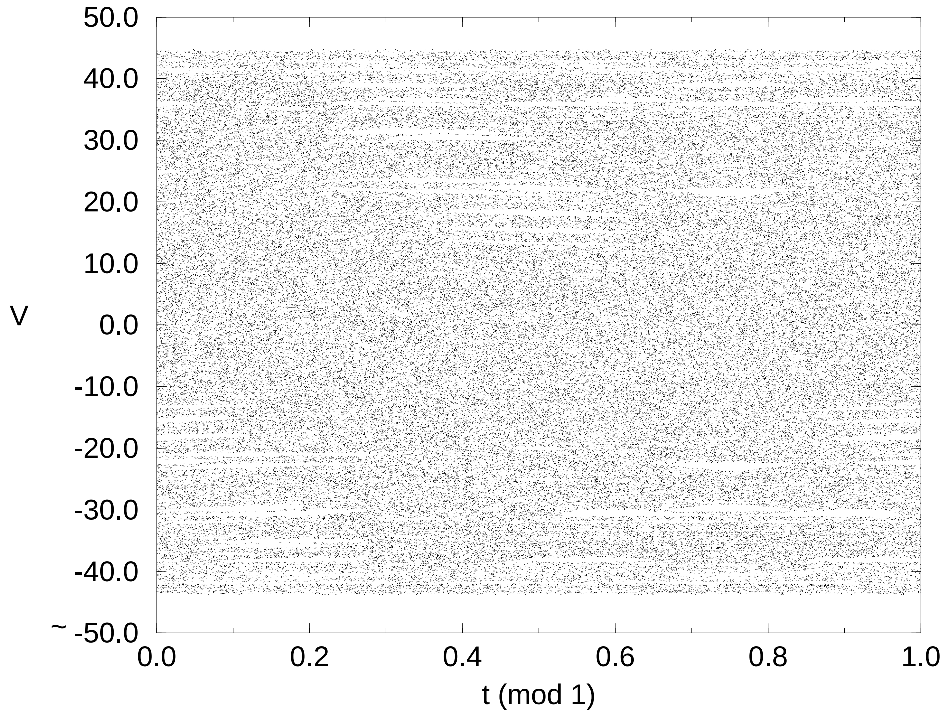

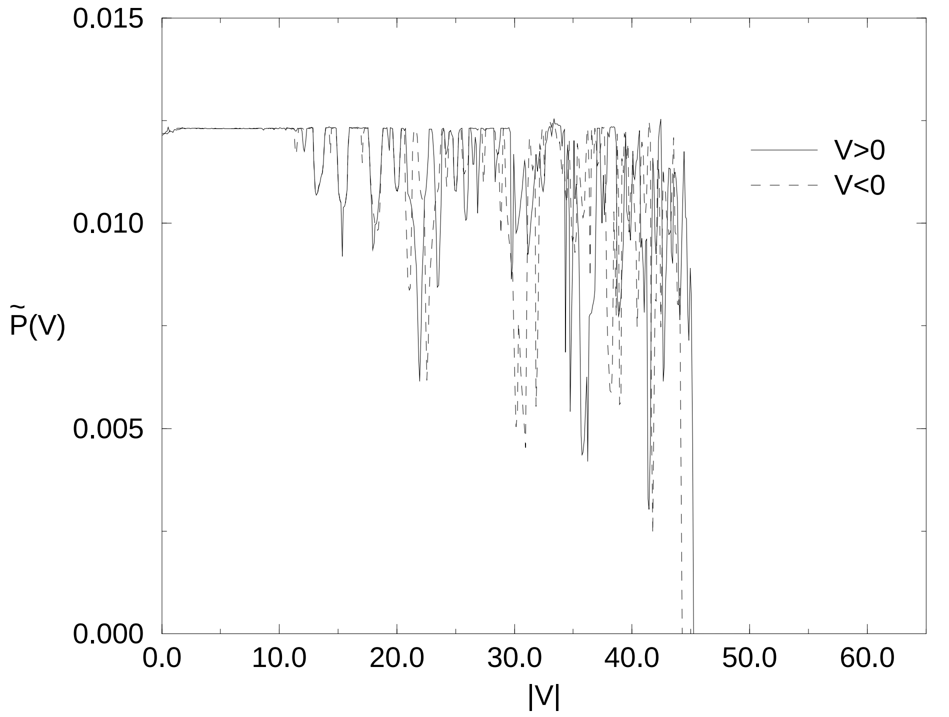

Figure 11.c: The available phase space Ω_{H_0} (top) and the corresponding probability density $\tilde{P}(V)$ (bottom) for $H_0 = 500$.

The main feature of the islands, demonstrated in these figures, is that they appear asymmetrically. In Ω, the available phase space of the Fermi map (3.1), the symmetry of the islands is established in one of two ways: The islands in some *chain* can appear in "pairs", i.e., in the same chain of islands there exist an island located around the point (V,t) and a "twin" island located around $(-V,t+\frac{1}{2})$ having the same shape. The other possibility is that there are two chains, each composed of the twins of the other. We call islands in the upper (lower) half of the phase space, $V>0$ ($V<0$), *positive* (*negative*) islands. If we initially place a trajectory inside an island, it will alternately move between islands in the upper and the lower half of the phase space. Hence, any chain in Ω, has the same number of positive and negative islands.

This symmetry is broken in Ω_{H_0}: A chain may include different numbers of positive and negative islands. Each island has a different shape, yet due to the area preserving property of the map (2.6), they all have the same area. (The boundary curves of the islands in some chain are mapped one into the other.) To demonstrate this symmetry breaking we introduce an example of some typical asymmetric chain. Taking $H_0=500$, Fig. 12 shows a chain of 3 islands encircling the (stable) 3-cycle

$$\vec{x}_0 \stackrel{\text{crossing}}{\longrightarrow} \vec{x}_1 \stackrel{\text{reflection}}{\longrightarrow} \vec{x}_2 \stackrel{\text{reflection}}{\longrightarrow} \vec{x}_0 \longrightarrow \cdots,$$

where

$$\begin{aligned}
\vec{x}_0 &= (V=21.691496772\ldots, t=0.749999999\ldots)\\
\vec{x}_1 &= (V=21.691496772\ldots, t=0.360101416\ldots)\\
\vec{x}_2 &= (V=-20.921389865\ldots, t=0.139898583\ldots).
\end{aligned}$$

(What is actually shown in Fig. 12 and in other figures in this chapter are three curves, each located in one of the islands, over which the trajectory moves if initial conditions are set inside one of the islands. We tried to set initial conditions close to the edge of the islands, so the resulting curves approximately draw the boundaries of the islands.) The arrows indicate whether the iteration between the points of the cycle is made by the sub-map of reflection or crossing. The Jacobian matrices of reflection and crossing are respectively

$$\mathbf{J}_{\text{ref}} = \begin{pmatrix} -1 & -2v_b\cos(2\pi t_n) \\ \text{sign}(V_{n+1})\frac{2\pi L}{V_{n+1}^2} & 1+2v_b\cos(2\pi t_n)\cdot\text{sign}(V_{n+1})\frac{2\pi L}{V_{n+1}^2} \end{pmatrix} \tag{5.1.a}$$

and

$$\mathbf{J}_{\text{cross}} = \begin{pmatrix} 1 & 0 \\ \text{sign}(V_{n+1})\frac{2\pi L}{V_{n+1}^2} & 1 \end{pmatrix}. \tag{5.1.b}$$

Substituting properly $\vec{x}_0$, $\vec{x}_1$ and $\vec{x}_2$ in these matrices and using the condition of linear stability (3.6), one can easily verify, in accordance to numerical observation, that the cycle is indeed stable.

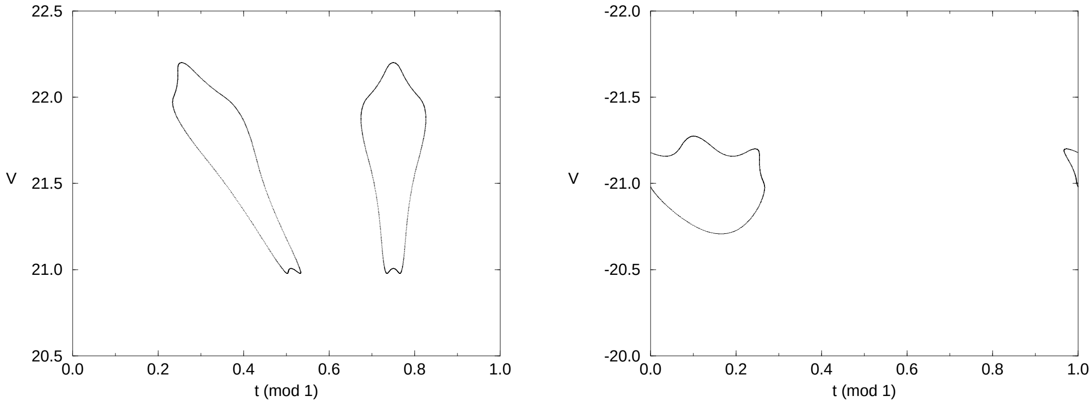

Figure 12: An example of an asymmetric chain of islands embedded in Ω_{H_0} for $H_0 = 500$. The chain is composed of two positive islands (in the upper half of the phase space, $V > 0$) and a single negative (in the lower half of the phase space, $V < 0$) island each having a different shape. What is shown here, are three curves, each located in a different island. Once the initial conditions are set over one of the curves, the trajectory jumps from a curve to another. The area each curve encloses is the same since the map (2.6) is area-preserving.

The random phase approximation (RPA) results (section 4.3) are not valid when islands appear since the entire area between $V_{\min}$ and $V_{\max}$ is not available anymore. The areas excluded from the upper half ($V > 0$) and the lower half ($V < 0$) of Ω_{H_0}, due to the existence of an asymmetric chain are different. For instance, for the chain introduced above (Fig. 12), the total area occupied by the two positive islands is twice as large than that occupied by the single negative one. This can be seen in Fig. 13 which shows the dips in $\tilde{P}(V)$, indicating the existence of this chain. The dip for $V > 0$ is two times bigger than that for $V < 0$.

The asymmetry of Ω_{H_0} is thus a combination of two "effects": The difference between $|V_{\max}|$ and $|V_{\min}|$ (Eqs. (4.6)) and the appearance of asymmetrical chains of islands. There is a major difference between these two effects. While $V_{\min}$ and $V_{\max}$ change continuously with H_0, the sudden appearance and disappearance of a chain of islands occurs at *bifurcation points.*[3] The value of $\langle d \rangle$, which is influenced by these two effects, is therefore a

[3]Bifurcation is the sudden change in the properties of a nonlinear system as a parameter is varied. In this case, the existence or the stability of a cycle are changed, leading to the appearance or the disappearance of the surrounding chain of islands.

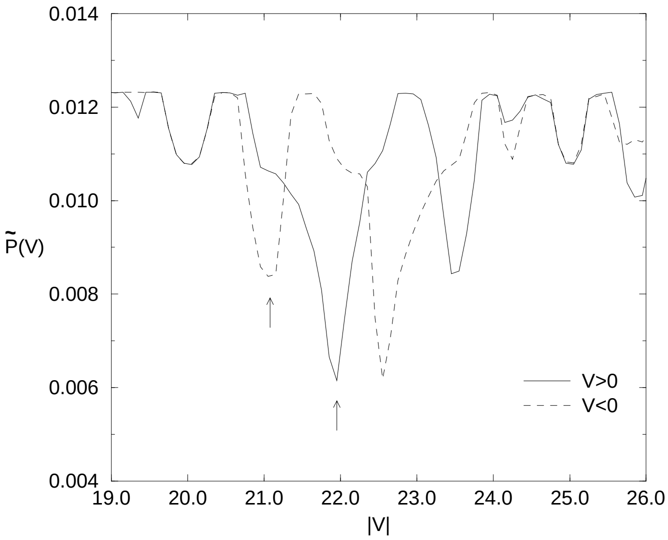

Figure 13: A magnification of the dips of $\tilde{P}(V)$ indicating the existence of the asymmetric chain shown in Fig. 12.

piecewise continuous function of H_0, discontinuous at these bifurcation points.

Fig. 14 shows the value of the mean displacement per collision , $\langle d \rangle$, computed for several values of H_0. One can see that the value of $\langle d \rangle$ coincides with the RPA result only for small values of H_0. However, for the few cases we have checked, the deviations from the RPA results at larger values of H_0 are minor. It seems fair to conclude that the overall effect of the islands embedded in Ω_{H_0} is relatively small and the RPA is a good approximation in the range of H_0 values shown in Fig. 14. In particular, $\langle d \rangle$ does not change its sign due to the appearance of islands in Ω_{H_0}, and the net motion is still directed from the left to the right for these H_0 values.

The situation is completely different if we start with initial conditions inside one of islands. The trajectory, in that case, "jumps" from one island to the other, when in each of the islands it is found over a closed curve (see section 3.3 about the regular character of the motion inside islands). The set of collisions and reflections, as depicted by the jumps between the islands, is the same as that of the cycle, surrounded by these curves (see an example earlier in this section). If the chain has n_1 positive ($V > 0$) and n_2 negative ($V < 0$) islands then

$$\langle d \rangle_{\rm IC} = \frac{n_1 - n_2}{n_1 + n_2} L. \tag{5.2}$$

(The subscript IC refers to the fact that this value of $\langle d \rangle$ corresponds to a motion over an

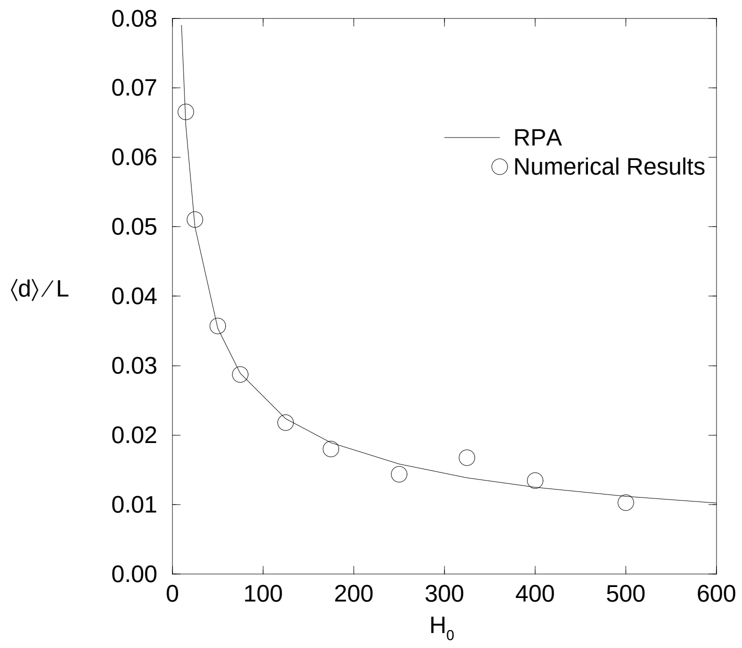

Figure 14: The value of $\langle d \rangle$ numerically computed for various values of H_0 (using Eq. (4.1) with $N \sim \mathcal{O}(10^9 - 10^{11})$), in comparison to the RPA results (Eq. (4.9)).

Islands' Chain). Comparing this to the value of $\langle d \rangle$ related to the motion in Ω_{H_0} we see a few important differences: The value of $\langle d \rangle_{\rm IC}$ must be rational. It is usually, at least for small n_1 and n_2, much larger than $\langle d \rangle$. For example, taking $H_0 = 500$, the chain shown in Fig. 12 is embedded in Ω_{H_0}. For the regular motion over this chain, $\langle d \rangle_{\rm IC} = \frac{1}{3}L \simeq 33.3$, while the corresponding value for the stochastic motion in Ω_{H_0} is $\langle d \rangle \simeq 0.01L = 1$, i.e, smaller by more than an order of magnitude. Moreover, in Ω_{H_0}, the velocity of the particle varies between $V_{\rm min}$ and $V_{\rm max}$. On the other hand, for the regular motion over a chain of islands, the speed of the particle does not change significantly during the motion and can be approximated by its initial value, $|V| \sim |V_0|$. The mean time interval between two consecutive impacts is smaller for the regular motion over the islands than for stochastic motion in Ω_{H_0}, since the latter includes long time intervals in which the particle's speed is low. Since both $\langle d \rangle_{\rm IC}$ is larger than $\langle d \rangle$, and $\langle \Delta t \rangle_{\rm IC}$ is smaller than $\langle \Delta t \rangle$, we conclude that the drift velocity, $\langle d \rangle / \langle \Delta t \rangle$, of a regular motion over a chain of islands embedded in Ω_{H_0} is usually much larger than that related to the stochastic motion in Ω_{H_0} itself. In other words, the efficiency of the mechanism is much larger when the motion is over a chain of islands than in Ω_{H_0}. However, the most significant difference between $\langle d \rangle$ and

$\langle d \rangle_{\mathrm{IC}}$ is that the latter can also be negative. If the chain includes more negative than positive islands then $\langle d \rangle_{\mathrm{IC}} < 0$ and the direction of the net motion is from right to left, opposite to the direction of the net stochastic motion. Fig. 15 depicts an example of such a chain.

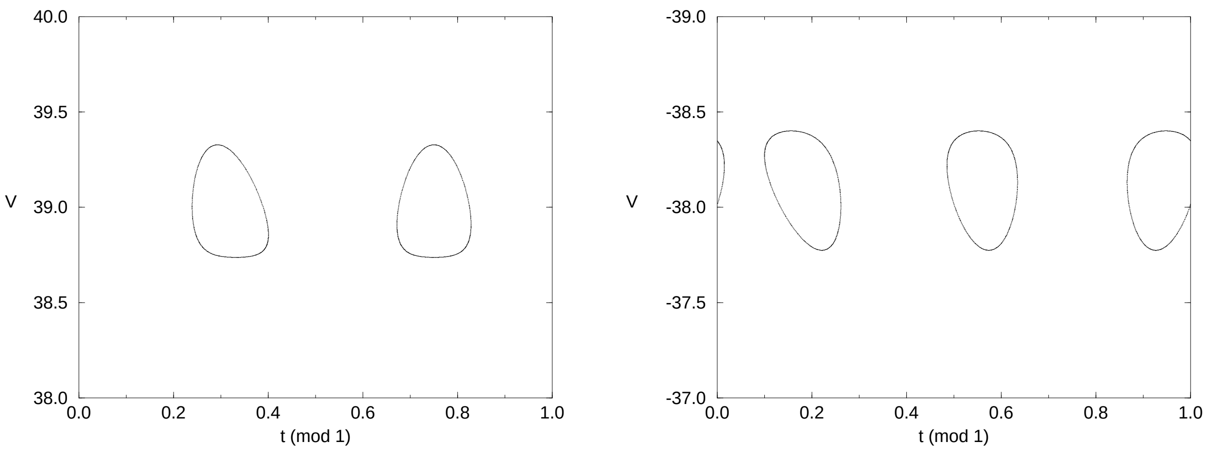

Figure 15: An example of an asymmetric chain of islands embedded in Ω_{H_0} for $H_0 = 500$. The chain is composed of two positive and there negative islands, which means $\langle d \rangle_{\mathrm{IC}} = -\frac{1}{5}L$.

5.2.2 Pseudo KAM Boundaries

We already know that the allowed velocity values are between $V_{\min}$ and $V_{\max}$ (section 4.2). Is it possible that within these bounds there are KAM curves that cannot be crossed? These curves, if they exist, divide the phase space into mutually inaccessible area of stochastic motion. In that case, the first KAM curve bounds the phase space which is available to a particle with low initial velocity, thus defining a narrower range for the allowed velocities. For the Fermi map (3.1) such a boundary KAM curve exists (chapter 3), whereas for the map (2.6) with finite H_0, KAM curves do not appear. The difference is because of the fact that a map should be sufficiently smooth for KAM curves to appear in its associated phase space (see section 3.3 about the KAM theorem). While the Fermi map is an analytic one, the map with a finite H_0 is discontinuous and therefore does not satisfy the conditions for the existence of KAM curves. However, numerical observations reveal an interesting phenomenon: for some H_0 values it looks as if curves which bound the available phase space do exist.[4] A trajectory of a particle in these cases will stochastically

[4]We observed this in all of the cases we have checked for H_0 between 1000 an 10000 and in few of the cases for H_0 between 100 and 1000.

explore only some part of Ω_{H_0}.

A more careful study of this behavior reveals that nothing bounds the motion in the phase space (except for the $V = V_{\min}$ and $V = V_{\max}$ boundaries, see section 4.2). It appears that if we iterate the map a sufficiently large number of times, then suddenly, usually after many iterations, the trajectory will cross the boundary of the sub-space it was trapped in and move to some other part of Ω_{H_0}. We therefore call these imaginary boundaries: pseudo KAM boundaries (PKB). Fig. 16 shows the phase space explored by the first $2 \cdot 10^{10}$ points of a trajectory of a particle given a low initial velocity. For $H_0 = 2500$, we expect to find the boundaries at $V_{\max} = 100.5$ and $V_{\min} = -99.5$, however, one can see that a PKB appears at $|V| \sim 63$, preventing the particle from being further accelerated.[5]

How do we explain this phenomenon? Let us investigate the PKB shown in Fig. 16 ($H_0 = 2500$, $|V| \sim 63$). Fig. 17 shows a chain of islands composed of $n_1 = 420$ positive (in the upper half of the phase space, $V > 0$) and $n_2 = 466$ negative (in the lower half of the phase space, $V < 0$) islands. (A chain composed of n_1 positive and n_2 negative islands will be referred to as an n_1–n_2 chain.) One can see that this chain looks very similar to the boundary of the area shown in Fig. 16, and at first glance it seems that this chain is the PKB. The chain indeed resembles a KAM curve: The islands, which are all very narrow, almost touch each other, with only small spaces between them. They look as if they are oriented along some imaginary KAM curve.

Consider a trajectory which moves very close to this chain from below. (We say the trajectory moves below the chain, although it alternates between the positive and negative branches of the chain, and with respect to the latter it actually moves from above.) Clearly, we expect to find strong phase correlations in the motion. If the trajectory passes very close below the chain, then for a certain number of the subsequent iterations, it moves close to the chain, i.e. over a narrow velocity band. In Fig. 18 we can see the 420–466 chain shown in Fig. 17 and a narrow stochastic layer below this chain. The trajectory moves over this stochastic layer for many iterations (Fig. 18 shows the first 25000 iterations of a trajectory initially placed close to the chain. They remained in the narrow layer). Usually, after a certain number of iterations, it falls back into the stochastic sea, but in some rare cases it escapes. In that sense, the structure of Ω_{H_0} just below the

[5] In comparison, the phase space plots shown in Figs. 11.a–c were completely explored after less than 10^8 iterations.

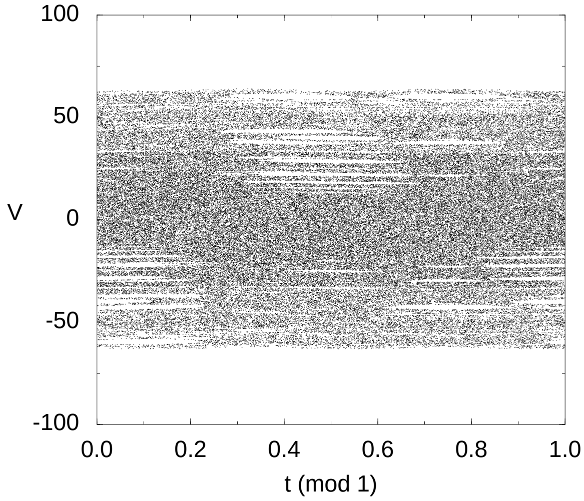

Figure 16: The subspace of Ω_{H_0} for $H_0 = 2500$ explored after $2 \cdot 10^{10}$ iterations of the map (2.6).

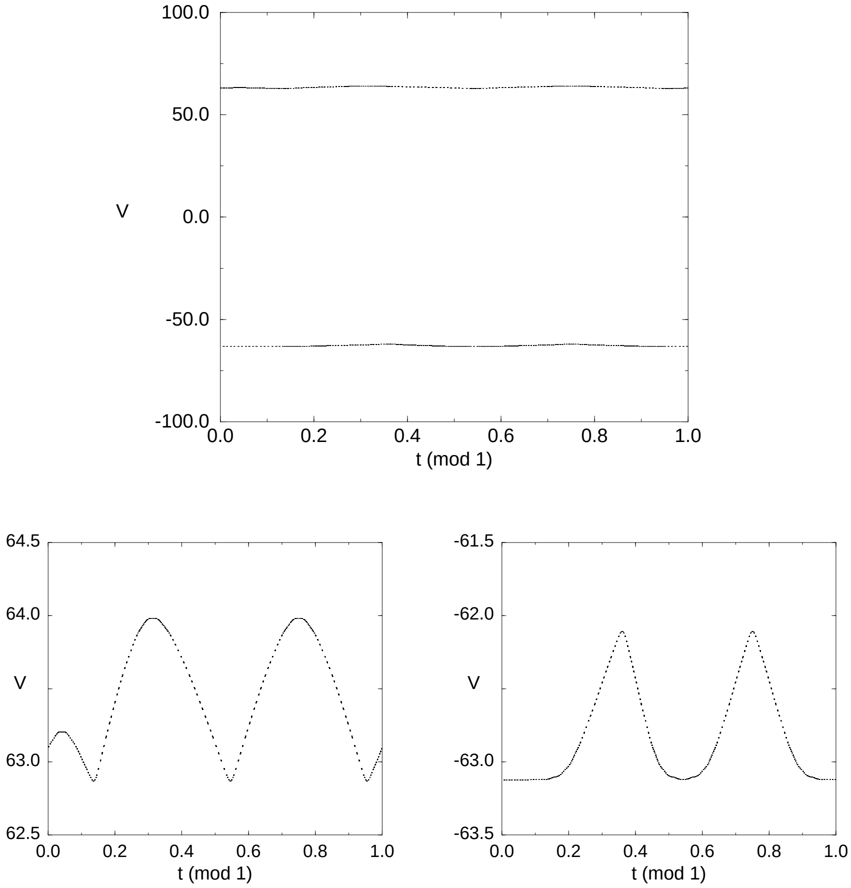

Figure 17: The 420–466 chain which appears in Ω_{H_0} for $H_0 = 2500$ at $|V| \sim 63$. Its shape resembles the boundary of the area shown in Fig. 16. The two figures in the bottom show in magnification the positive (left) and negative (right) velocity branches of the chain.

420–466 chain resembles the structure of Ω just below the first KAM curve. In both cases although the motion is stochastic, it is strongly correlated and only gradually deviates from the boundary. The difference is, of course, that while a KAM curve is a perfect boundary, the chain will eventually be crossed. Numerical simulations show, in general, that the closer a trajectory gets to the chain the larger is the escape probability. The trajectory, stochastically moving in Ω_{H_0}, occasionally gets very close to the chain until at one of the times it finds its way out.

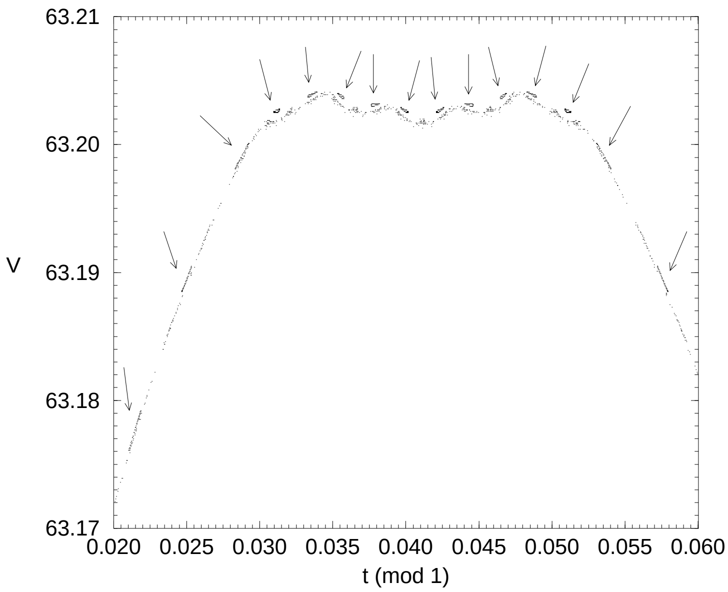

Figure 18: The 420-466 chain (the arrows point at the islands of the chain), which appear in Ω_{H_0} for $H_0 = 2500$. A narrow stochastic layer appears restricted below the islands . The motion over this narrow layer can take place for thousands of iterations. Note that only a small part of the positive velocity branch of the chain is shown here.

This is however not the whole picture. Fig. 19 depicts an extended picture of the phase space in the vicinity of the 420–466 chain. We can see that over a small region of the phase space there are several other chains which are all located very close to each other.[6] Since the motion near a chain of islands is phase correlated, a trajectory that moves close to a chain will propagate along it, while gradually moving away. If there are many chains over a small area of Ω_{H_0}, then while the trajectory moves away from one chain it gets closer to another, along which it propagates for subsequent iterations. This is an over-simplified picture since it is not always possible to relate the motion to a

[6]Fig. 19 shows only the largest and the most dominant chains in this region.

particular chain at each instance, however, it roughly explains why a trajectory mainly propagates along the chains and only slowly moves from one chain to another. The narrow area around the chains is a band of stochastic motion, where the trajectory is trapped for some iterations each time that it gets there. The 420-466 chain is only the final member of a set of chains embedded in that band. If the trajectory crosses this chain it will escape to another subspace of Ω_{H_0}. However, the trajectory does not usually reach this "final chain" at all. It wanders through the band between the chains, and usually falls back into the stochastic sea before it succeeds to pass through all the chains. It is therefore the whole set of (close to each other) chains which we should refer to as the PKB and not just the final member of this set.

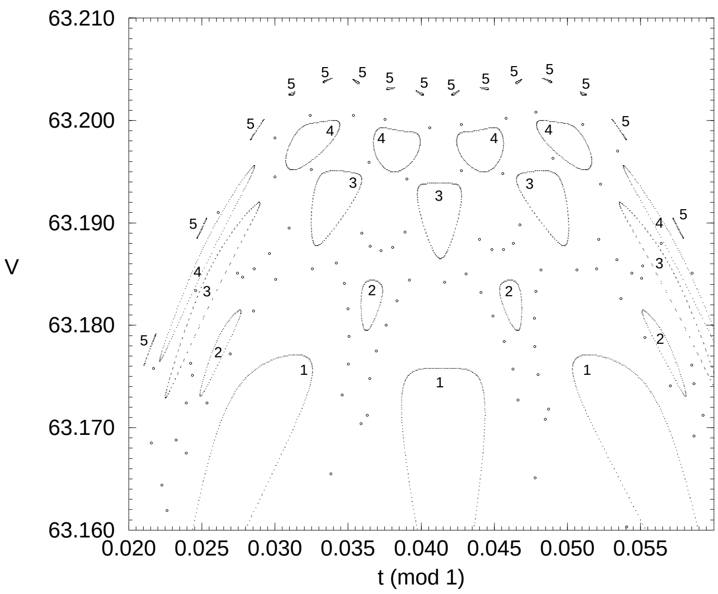

Figure 19: A few chains of islands located in a small area of Ω_{H_0} for $H_0 = 2500$ which form together a PKB. The numbers inside the islands indicate to which of the following chains they belong: 1) 27–33 ; 2) 37–47 ; 3) 49–59 ; 4) 60–72 ; 5) 420–466. The dots show a stochastic trajectory wandering between these islands. (Only a small part of the positive velocity branches of the chains is shown here.)

Few additional remarks should be made. First, a PKB is a bi-directional boundary: it bounds the lower part of Ω_{H_0} from above, but also bounds the upper part from below. Fig. 20 demonstrates how a trajectory which passes very close to the 420–466 chain from above, does not cross it. Second, we usually do not find only one but a few PKBs in Ω_{H_0}. The motion in Ω_{H_0} is thus bounded between two PKB until it crosses one of them and moves to some other subspace. For example, for $H_0 = 2500$ we found different PKBs appearing at the following speed values: $|V| \sim 25, 34, 49, 56, 64, 71, 79, 88 \ldots$. Above the PKB at $|V| \sim 88$ the motion is so strongly correlated that many PKBs appear close to each other. Comparing the different PKBs we find that some of them are easily crossed while others can be a "tough nut to crack". Third, the appearance of PKBs does not contradict the ergodicity assumption. One just has to iterate the map a large number of iterations, a few orders of magnitude larger than the number needed to cross each of the PKBs. An extended discussion of this issue is given in Appendix A.4.

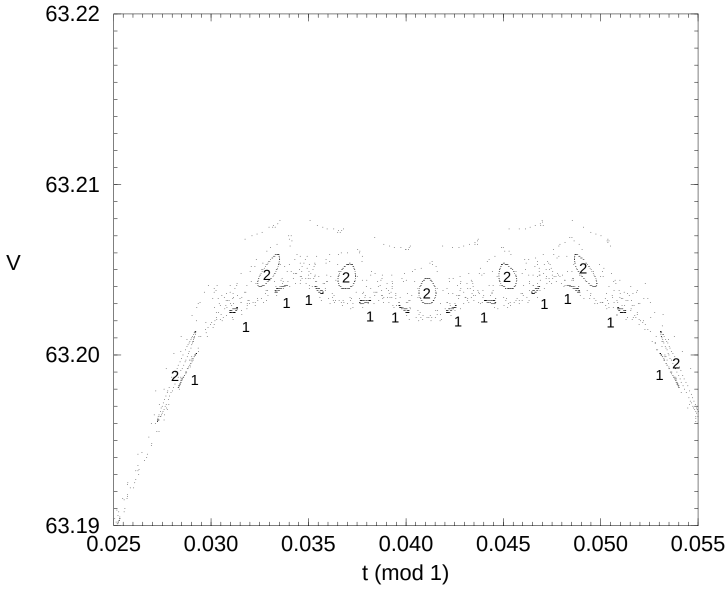

Figure 20: The 420–466 chain (1), a 157-164 chain above it (2) and a narrow band of stochastic motion in which they are embedded. This is the upper side of the PKB shown in Fig. 19. (Only a small part of the positive velocity branches of the chains is shown here.)

We have shown that long and narrow chains of islands, which surround parts of the available phase space, serve as pseudo KAM boundaries (PKBs). At the vicinity of these chains, which usually appear in groups, close to each other, the motion is strongly correlated. A trajectory stochastically wanders between the islands. It propagates along the chains and slowly moves from the one to the other. In order to move to another part of the phase space, the trajectory has to cross all the chains which form the PKB. However, due to the phase correlations this happens infrequently, only after many attempts. Figs. 21 and 22 give another example for a PKB, appearing at $|V| \sim 33$ when $H_0 = 3000$. This PKB is weaker than one discussed above (the $|V| \sim 64$, $H_0 = 2500$ case), i.e., less iterations are usually needed before it is crossed. This is probably because the chains of the latter are denser (the spaces between the islands are smaller) and therefore the chains look and behave more like KAM curves. This is true in particular with respect to the final chain in this PKB, the 420–466 chain (see Fig. 17).

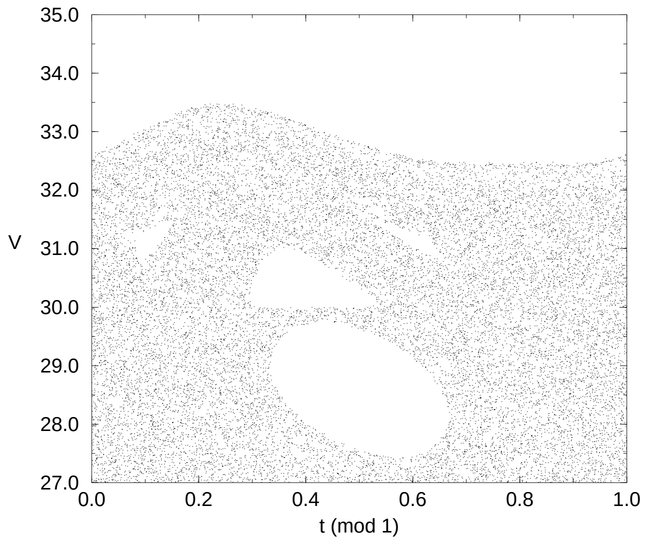

Figure 21: The motion in Ω_{H_0} for $H_0 = 3000$, bounded by a PKB at $|V| \sim 33$.

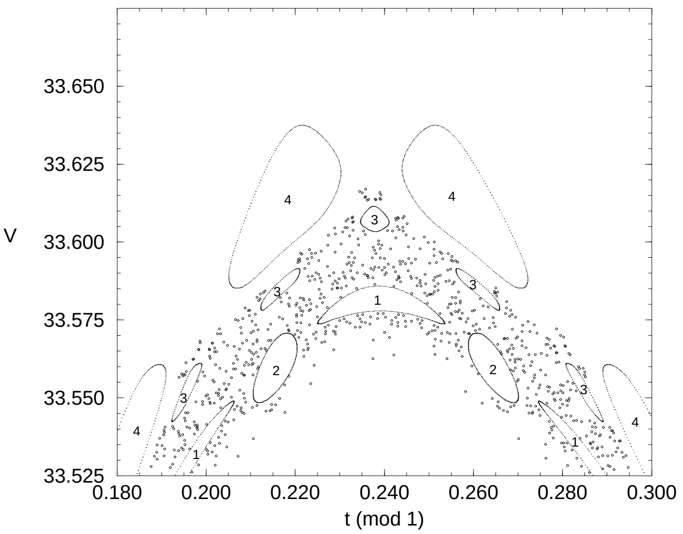

Figure 22: A few chains of islands located in a small area of Ω_{H_0} for $H_0 = 3000$ which form together the PKB appearing in Fig. 21. The numbers inside the islands indicate to which of the following chains they belong: 1) 13–10 ; 2) 13–11 ; 3) 27–21 ; 4) 14–11. The dots show a stochastic trajectory wandering between these islands. (Only a small part of the positive branches of the chains is shown here.)

6 Conclusions

In this work we have studied the properties of a dynamical map, which is a generalization of the celebrated Fermi accelerator map. While the Fermi map serves in the literature as a model for the stochastic acceleration mechanism, the "generalized" map is used in this work to model stochastic directed motion.

The map describes the motion of a particle in a one-dimensional asymmetric potential, periodic in time and space. Such systems were studied by several authors, however, most of them considered non-equilibrium kinetics and not deterministic motion. In other works ([8], for example) deterministic motion was considered, but using linear differential equations which do not yield stochastic motion. The system discussed in this work is therefore specialized in being both deterministic and non-linear stochastic. The main feature of all these systems, including the one discussed in this work, is, however, the same: The motion of the particle is, on the average, directed and characterized by some net drift velocity.

Numerical considerations led us to conclude that the motion is ergodic over some phase space, Ω_{H_0}. This is an important property since it indicates that the mean quantities of the motion are independent of initial conditions in Ω_{H_0}. It allows us to replace the time averages of the motion by the space averages over the available phase space, whose structure we have therefore aimed to explore. The equilibrium invariant distribution over this phase space is constant since, as we have proven, the map is an area preserving one.

The average height of the potential barriers, H_0, was chosen as the control parameter of the problem. All other parameters, like v_b, the maximal barriers speed, or L, the distance between neighboring barriers were held constant. We then tried to see how $\langle d \rangle$, the mean displacement of the particle per collision, is changed as a function of H_0. This quantity characterizes the average directed motion, and is related to the drift velocity by Eq. (4.4). The drift velocity itself cannot be calculated since the map is a simplified one and does not describe a real physical problem at low speed values. (In Appendix B we try to resolve this problem and estimate the behavior of V_{drift} as a function of H_0.)

Roughly speaking, we have shown $\langle d \rangle$ (and also V_{drift}) is a decreasing function of H_0 which is always positive, i.e, the motion is always directed in the same preferred direction. When H_0 is sufficiently low, the results coincide with those obtained by neglecting the deterministic process and randomly choosing the phase of the barrier's motion at the moment of impact. Phase correlations appear when H_0 is increased, since the particle can reach higher speeds and the time interval between two consecutive collisions decreases to the order of τ, the period of barriers' motion. Phase correlations are important for two reasons:

1. Modifications of the RPA (Random Phase Approximation) results, which are minor, at least over the range of H_0 values investigated in this work.
2. The appearance of pseudo KAM boundaries, which for long time intervals, bound the motion in some subspace of the available phase space.

The value of $\langle d \rangle$ was found to be of the order of a few percents of L, the distance between two neighboring barriers. A much better efficiency, i.e., a larger value of $\langle d \rangle / L$, is obtained if the particle's initial conditions are inside one of the islands embedded in the phase space. The motion of the particle in that case is regular, non-stochastic, composed of a repeating set of reflections and crossings. Each chain is thus characterized by its $\langle d \rangle$ value, and at a given H_0 (above some threshold value) one can find chains with either positive or negative $\langle d \rangle$. This means that a directed regular motion of high efficiency can be achieved in both directions, provided that initial conditions are properly set.

The dependence of the motion on other parameters of the system, may serve as a subject for further research. One may study the behavior of $\langle d \rangle$ as a function of v_b (for various values of H_0). The parameter v_b characterizes the asymmetry of the system and its stochasticity. The difference of the threshold speeds for crossing a barrier from the left or the right increases linearly with v_b (see Eq. (2.4)), and therefore, large v_b corresponds to highly asymmetric systems. The system is also highly stochastic when v_b is large since the speed of the particle changes rapidly and phase correlations become weaker. Respectively, small values of v_b correspond to "almost" symmetric systems with a more ordered behavior.

The effect of a small thermal noise on the system may also be considered. In principle, the addition of a random component to a deterministic system, should destroy the special structure of the phase space. However, if the noise is very small compared to the kinetic energy of the particle, then the characteristic time for completely losing the "footprints" of the old phase space can be considerable and on smaller time scales, some interesting phenomena might be observed. One may check the possibility of thermal noise to trigger a trajectory into and out of an island, or the effect of thermal noise on the boundaries of the phase space.

Finally, the appearance of pseudo KAM boundaries (PKB) seems to be an interesting phenomenon which requires a detailed study. Similar behavior is found if a KAM torus is destroyed when nearby islands increase and break through it. It is then called a *cantorus* (see [27], section 3.9). We have shown in this work that pseudo barriers may be observed even if KAM tori do not exist. This is especially relevant for discontinuous maps in which KAM tori are forbidden.

Appendix A Numerical Considerations

A.1 General

Investigating a dynamical system is a combination of analytical and numerical work. This appendix deals with the problems related to the numerical process with an emphasis on the system described in this particular work.

The evolution of the system, described in section 2.2, is given in terms of a mapping (2.6). A computer was used to perform the iterations and plot the resulting trajectories. These plots were then used to study the properties of the map. The numerical process, thus, consists of three steps: iterating, plotting and observation. Each step has its own level of precision:

1. The precision of numerical calculations: Throughout this work we used a precision of 16 significant digits ('double precision') in our numerical calculations.

2. The resolution of the plots: We used a standard plotting program which creates plots at a resolution of 6 significant digits.

3. The resolution of observations: One should consider the fact that while observing plots of different trajectories, the human eye can notice details only at a resolution of 2–3 significant digits.

A.2 Roundoff Errors

Chaotic systems are characterized by their "sensitive dependence on initial conditions", i.e, by the fact that nearby trajectories diverge exponentially fast with time (section 1.1). A quantity that measures the (mean) exponential rate of divergence of nearby trajectories are the *Lyapunov exponents* (LE). (See [18] section 5.2b, for definitions of the LE and further references.) Roughly speaking, an N-dimensional system is chaotic if at least one of the N exponents is positive. For conservative systems the sum of LE is zero, which means that an area preserving map is stochastic if, and only if, one of its two exponents is positive. The sensitive dependence on initial conditions makes it impossible to compute a trajectory in chaotic systems since *roundoff errors*, due to the finite precision of numerical calculations, will be exponentially amplified with time, and the computed trajectory will soon lose any resemblance to the "real" one. This is indeed the situation concerning the motion in the phase space of the map (2.6). In fact, the dynamics described by the map (2.6) have an additional feature which brings about the divergence of nearby trajectories. We refer to the fact that it is discontinuous in the phase space over the two curves $|V - v(t)| = \sqrt{2H(t)}$ which represent the critical conditions for crossing a barrier (Fig. 8). One should consider a scenario that because of numerical errors, a trajectory would fall at the "wrong" side of a discontinuity curve. If this happens, then on the next iteration the computed trajectory will be mapped by the wrong sub-map (either of crossing or of reflection, see Eq. (2.6.a)) and lose any relation to the "real" one.

However, although we fail to calculate a single trajectory, still the main features of the stochastic motion are not affected by the (exponentially magnified) roundoff errors. The computed trajectory describes a motion which is 'area-filling' over the available phase space at a constant equilibrium invariant distribution. One can simply regard the "numerical motion" (the map together with the rounding process) as a mapping defined over a dense grid with a spacing equal to numerical precision. The "new" map is an area preserving one, where the area is measured in terms of the number of mesh points. The image of each mesh point is hardly affected by the rounding process, and therefore the structure of the available phase space is not deformed. Thus, although the trajectories are completely changed due to roundoff errors, the structure of the available phase space and the equilibrium invariant distribution stay the same. (The fact that the phase space is composed of a set of discrete mesh points cannot be seen since numerical precision is much higher than plotting or observation resolutions.) Fortunately, we are not interested in the individual trajectory but in the statistical properties of the motion which are derived from the picture of the phase space and the related probability density.

Concerning regular motion, the situation is even simpler. While plotting two neighboring regular trajectories, we usually find that the obtained curves neither diverge from nor converge into each other and this means that one of the LE vanishes. But, since their sum is zero, it follows that the other one vanishes too. Therefore, not only that numerical calculations produce a correct picture of regular curves, but they also describe properly the motion over these curves. Deviations of trajectories over regular curves increase only linearly with time. Using a precision of P significant digits in numerical calculations ($P = 16$ throughout this work), two neighboring regular trajectories become separated after $n_{\max} \sim \mathcal{O}(10^P)$ iterations, while two neighboring stochastic trajectories diverge within $n_{\max} \sim \mathcal{O}(P)$ iterations.

The difference between the values of the LE, related to a regular or a stochastic motion, is best seen in the vicinity of periodic points. Let $\vec{x}_0$ be a periodic point of period n of the map T. Let L be the map obtained by linearizing T^n in the vicinity of $\vec{x}_0$ (which is a fixed point of T^n).[1] There is a simple relation between, λ_i, the eigenvalues of L, and σ_i, the LE characterizing the motion at the vicinity of $\vec{x}_0$, given by

$$\sigma_i = \ln |\lambda_i|. \tag{A.1}$$

This can be easily understood in the following way: One can choose $\vec{w}$, the deviation of initial conditions from the fixed point $\vec{x}_0$, to be an eigenvector $\hat{e}_i$ of L. For $\vec{w} = \hat{e}_i$, $L^m \hat{e}_i = \lambda_i^m \hat{e}_i$, and therefore: $\sigma_i(\hat{e}_i) \equiv \lim_{m\to\infty} \frac{1}{m} \ln \|L^m \hat{e}_i\| = \ln |\lambda_i|$. In the vicinity of an elliptic fixed point of a 2-dimensional map, the motion is regular over ellipses encircling the point. The eigenvalues of the linearized map are $\lambda_{1,2} = e^{\pm i\alpha}$, which means that $\sigma_{1,2} = 0$. On the other hand, in the vicinity of a hyperbolic fixed point, the motion is stochastic on one or both branches of a hyperbola. The eigenvalues of the linearized map are $\lambda_1 = \lambda$ and $\lambda_2 = \frac{1}{\lambda}$ (where λ is real), and therefore $\sigma_{1,2} = \pm \ln |\lambda|$, which means that one of the exponents is positive unless $\lambda = \pm 1$. For $\lambda = \pm 1$, the fixed point is marginally (un)stable and the motion diverges from the fixed point over straight lines, at a linear rate.

A.3 Determination of Ergodicity

In section 4.1 we have suggested that the map (2.6) describes an ergodic motion in the available phase space Ω_{H_0}. We based this argument on the fact that the same picture of Ω_{H_0} was obtained regardless of initial conditions (unless initial conditions lead to a regular motion). We then claimed that this indicates that the system is indecomposable, i.e., ergodic. However, one should consider a few problems in using numerical tools to determine ergodicity

The plots of the available phase space Ω_{H_0} have finite resolution. One cannot neglect the possibility that at a finer resolution, the picture does depend on initial conditions.

[1] In matrix form $L\vec{x}_n = \vec{x}_{n+1}$, where the matrix L is the product of the n Jacobian matrices, evaluated at the points of the n-cycle of T: $L = \prod_{i=0}^{n-1} \mathbf{J}(T^i(\vec{x}_0))$.

(The relevant resolution is the coarser of the two resolutions: that of the plotting program and that of the human eye.) Therefore, the best conclusion concerning our system, is that there are no sub-space elements which are invariant with respect to the mapping and have a linear scale which is larger than the resolution, η. The concept of ergodicity refers to the limit when η vanishes, however if η is sufficiently small, it is reasonable to assume that the motion is indeed ergodic. Yet, the fact that only details above some resolution level are observable, might be misleading in some cases. An example of such a case was shown when we discussed the Fermi map. The probability density of finding the particle with a velocity V between two collisions, $\tilde{P}(V)$ (Fig. 5), reveals the existence of two, and possibly more, small islands at a velocity of about 11, which were not observed by looking at the phase space plot (Fig. 4). Anyhow, since these islands are small, their influence (on the value of the net drift velocity, for instance) is small. Generally speaking, one usually tries to learn about the general qualitative properties of the system by looking at the phase space plots, and for this purpose the (relatively) low resolution suffices. In order to derive quantitative results, like the drift velocity, one has to use numerical calculations of higher precision.

Another problem, related to the determination of ergodicity, originates from the finite precision of the calculation (roundoff errors). These errors can be considered as a sort of a "noise" which allows trajectories, originally moving over a certain invariant set in the phase space, to move to another set. A decomposable system then might seem to be ergodic. One should remember that the boundary of an invariant set is a KAM curve. If this curve separates between two sets of stochastic motion, then numerical noise destroys it and a transition between the sets is possible.[2] In this work the situation is different since the boundary curves of the stochastic sea separate it from regions of regular motion. All the regular curves which lie at a distance smaller than the precision, ϵ, from the boundaries are destroyed by the numerical noise and become a part of the stochastic sea.

[2]One would still be able to notice this transition and to conclude (or at least suspect) that there is a numerical problem there. Because of numerical noise there is an overlap between the two sets in a narrow band of a characteristic width ϵ (representing the numerical precision). A trajectory has to enter this overlap region in order to make the transition between the sets. The observed sets are of a characteristic size η (the resolution) or more. Assuming that the motion (including the numerical noise) is at a uniform probability density over each of the sets and that $\epsilon \ll \eta$, one can easily conclude that the trajectory would have to go through many iterations ($\geq \mathcal{O}(\frac{\eta}{\epsilon})$) in one the sets before making the transition to the other. This resembles a pseudo KAM curve in the sense that the trajectory stays for a long time in a certain region of the phase space and then suddenly makes a transition to another region, where it again remains for a long time. However this is a "numerical phenomenon", while a pseudo KAM curve is a real feature of the dynamics.

On the other hand, as discussed in section A.2, if a regular curve lies deeper within the region of regular motion, then it is not severely affected by roundoff errors. Therefore, roundoff errors add bands of width ϵ to the boundaries of the stochastic sea. However, these bands cannot be observed since the numerical precision is much better (by several orders of magnitude) than the resolution of observations.

A.4 Time-Averaging

The ergodicity hypothesis assumes that in the course of time, any trajectory explores the entire available phase space and eventually covers this region with some distribution given by $\tilde{P}(\vec{x})$, which is constant for conservative systems (see section 3.2). The averages of observable functions can thus be computed by averaging either over time or over space (Eqs. 4.1 and 4.2). Throughout this work, we use the first option of time averaging. When using this approach, one has to decide how many iteration of the map are needed before results are obtained with a satisfying accuracy. It appears that due to features of the motion, this number can be much larger for some values of the control parameter than for others.

The existence of a pseudo KAM boundary (PKB) is an example for a case in which a relatively large number of iterations is needed before the trajectory explores the entire available phase space, Ω_{H_0} (see section 5.2.2 about this phenomenon). On smaller time scales, the motion is trapped within some subspace of Ω_{H_0}. However, one can still try to characterize the motion inside a pseudo bounded subspace, which is, similar to the motion in the whole phase space, ergodic with a constant equilibrium invariant distribution. The motion can be time averaged using a long trajectory which does not escape from the subspace. In fact, we computed these averages for different subspaces and found, even for the same values of the control parameter, H_0, examples with both positive and negative values of $\langle d \rangle$, the mean displacement per collision of the particle. This means that if PKBs which divide Ω_{H_0} into several subspaces exist, then the motion is composed of long intervals which are (on the average) directed either form the left to right or vice versa. However, when performing time averages over the motion in some subspace of Ω_{H_0} one should consider the following "boundary" problem: The boundaries of a subspace are not well defined. A PKB is composed of a few chains. One might expect the last of them to be the boundary of the subspace. However, when getting close to the boundary, a trajectory does not usually pass all the chains and therefore the values of $\tilde{P}(V)$, the probability density of finding the particle with velocity V between two collisions, may be under-estimated right below the last chain. On the other hand, as also mentioned in section 5.2.2, the trajectory can be trapped for long interval in a narrow stochastic band near the boundaries, moving between the chains. This, in turn, can lead to an over-estimate of $\tilde{P}(V)$ at the boundary. This is not a numerical problem, it has a physical meaning. It means that the motion in a subspace bounded by PKB can be characterized only if most initial conditions in the subspace lead approximately to the same time-averages. This happens only if the pseudo boundaries are relatively strong, so that a typical trajectory reaches the boundary band many times before it escapes. In that case one can expect the motion near the boundary to be properly weighted.

A similar boundary problem occurs near the phase space $V_{\rm min}$ and $V_{\rm max}$ velocity bounds (section 4.2). A particle which moves with a velocity close to these values, will be reflected, thus changing its velocity, only if it collides with a barrier at some small interval of phases around $t = \frac{1}{4}$. The particle can undergo many collisions before this happens. In the meantime, the motion of the particle in the phase space will be over the torus $V =$ const. When the particle will eventually be reflected, its new velocity will still be relatively high, so for a number of iterations, it will again move over a torus. The trajectory is thus composed of intervals of motion in which the particle's velocity is constant. In order to obtain a good estimate of $\tilde{P}(V)$, the number of iterations should be much larger than any of these intervals. The lengths of these intervals become larger and tend to infinity when the velocity approaches $V_{\rm min}$ or $V_{\rm max}$, however, since we use some finite resolution along the V-axis, we do not have to reach these values but only get close to them. For example, the probability densities, $\tilde{P}(V)$, shown in Figs. 11.a–c and the numerical results shown in Fig. 14 were computed using a resolution of $\Delta V = 0.1$ along the V axis. We needed an order of magnitude of 10^9–10^{10} iterations to obtain these results. Using a smaller number of iterations usually led to either an over-estimate or an under-estimate of $\tilde{P}(V)$ close to these boundaries.

Appendix B The Exact Problem

The map (2.6) does not give an exact description of the dynamics. It makes the non-physical assumption that the barriers do not change their position but nevertheless, when the particle hits one of them, they behave as if their velocity is given by some periodic function. This assumption simplifies the calculations since the particle goes through only a single collision with the barrier and then travels exactly a distance L until it collides with another neighboring barrier. How are the results modified if we use the "exact" map, in which the motion of the barriers is considered? In chapter 5 we see the invariant probability densities $\tilde{P}(V)$ obtained for several values of H_0. A common feature to all of them is their low speed behavior: for $|V|$ smaller than some threshold value, $U_s(H_0)$, $\tilde{P}(V) = \text{const} \neq 0$. This, in turn, leads to the vanishing of V_{drift} (see Eqs. 4.3 and 4.4). We claim that this is a result of the use of a "simplified" map which is a bad approximation when the speed of the particle, $|V|$, is of the order of v_b, the barriers' maximum velocity, or less.

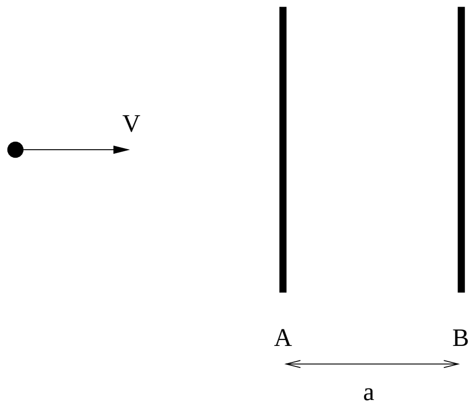

Figure 23: The exact problem: The barrier oscillates between the points A and B. The particle may undergo several collision with the barrier before leaving the interval A–B.

We distinguish between the following three cases:

1. $|V| \gg v_b$. The use of the simplified map is well justified in this case if we also assume that $L \gg a$, where L is the spacing between the barriers and a is the amplitude of the barriers motion. (This is indeed the case in this work since $L = 100$ and $a = \frac{1}{4\pi}$.) This was shown explicitly for the Fermi map in Ref. [14], however, the same reasoning holds here: Since $|V| \gg v_b$, the particle goes through only a single collision each time it collides into a barrier and since also $L \gg a$, the moment of impact is only slightly modified if we consider the motion of the barriers. The speed of the particle after a collisions also

satisfies $|V| \gg v_b$.

2. $|V| \sim v_b$. This is probably the most difficult case to handle using the exact map. The barrier is moving between points A and B. Since $|V| \sim v_b$, the particle may undergo several collisions with the same barrier before being reflected to another, i.e., before leaving the interval between the points A and B (Fig. 23). Moreover, the motion of the barriers becomes an important factor in determining the moment of impact. However, once the particle was finally reflected to another barrier, the chances are that its new speed also satisfies $|V| \sim v_b$ because $|V|$ cannot become much larger than v_b as a result of a few collisions with the same barrier. On the other hand, if $|V|$ becomes much smaller than v_b after a certain collision, then the particle will move so slowly that before leaving the interval between A and B, a second collision with the same barrier will probably occur, and it will regain a new speed $|V| \sim v_b$. This is the major difference between the exact problem and the simplified one, in which the particle's speed may become very small after a single collision. Generally speaking, the lower the speed that the particle acquires after a collision with a barrier, the lower the probability that it will succeed in leaving the interval A–B without being accelerated due to a second collision with the barrier. Therefore, near $|V| = 0$, $\tilde{P}(|V|) = \tilde{P}(V) + \tilde{P}(-V) = 2\tilde{P}(V)$ is a decreasing function of $|V|$.[1] In particular, while dealing with the exact map, the velocity of the particle cannot vanish, and therefore $\tilde{P}(0) = 0$ and since since we don't see any particular reason why $\tilde{P}(|V|)$ would not be a continuous function of $|V|$, we conclude that for the exact map $\tilde{P}(|V|) \to 0$ when $|V| \to 0$.

3. $|V| \ll v_b$. To complete the last argument, let us see what happens if the speed of the particle becomes somehow very small. The barrier is oscillating between the points A and B while the particle slowly approaches point A (Fig. 23). The probability that it will collide with the barrier while the last is just leaving point A is very small, and it decreases to zero when $|V|$ approaches zero. It is more likely that the particle will propagate very little beyond the point A and then collide with the barrier incoming from point B, thus being accelerated. We see that the probability of a very slow particle to be even more decelerated, vanishes when $|V|$ vanishes. This agrees with the above conclusion that $\tilde{P}(|V|) \to 0$ when $|V| \to 0$.

[1] When $|V| \simeq 0$, the probability that the particle crosses a barrier is very low and the map (2.6) can be treated as the Fermi map. However, for the Fermi map $\tilde{P}(V) = \tilde{P}(-V)$ (see section 3.2). In fact, the arguments introduced in this appendix are valid for all H_0 values, including $H_0 = \infty$.

The drift velocity does not vanish if $\tilde{P}(|V|) \to 0$ when $|V| \to 0$. In order to obtain a rough estimate of how $V_{\rm drift}$ depends on H_0 we take the random phase approximation (RPA) (section 4.3) results and see how they are modified. The invariant probability density $\tilde{P}^{exact}(V)$ (for the exact problem) differs from $\tilde{P}^{simplified}(V)$ (for the simplified problem) only when $V \leq \mathcal{O}(v_b)$. The upper limit in the integrals in Eqs. (4.2)–(4.4) changes proportionally to $\sqrt{H_0}$ (Eqs. (4.6)). If $\sqrt{H_0} \gg v_b$, then $\langle d\rangle_{\rm RPA}$, the mean displacement per collision of the particle, is slightly modified:

$$\langle d\rangle_{\rm RPA}^{exact} = \frac{v_b L}{2\sqrt{H_0}}[1 + \mathcal{O}(\frac{v_b}{\sqrt{H_0}})] \tag{B.1}$$

(Compare this with Eq. (4.9).). The average time interval between two consecutive collisions (with different barriers) does not diverge in this case. Its value has the form

$$\langle \Delta t\rangle_{\rm RPA}^{exact} = \frac{L\ln(2\sqrt{H_0})}{2\sqrt{H_0}}[1 + \mathcal{O}(\frac{v_b}{\sqrt{H_0}})] + \frac{L}{2\sqrt{H_0}}[1 + \mathcal{O}(\frac{v_b}{\sqrt{H_0}})]\, f(v_b), \tag{B.2}$$

where $f(v_b)$ is some function of v_b, which for $v_b \ll 1$, can be approximated by $f(v_b) \simeq \ln(v_b)$.[2] Dividing these two quantities, we find that the drift velocity is given by:

$$V_{\rm drift}^{exact} = \frac{v_b}{\ln(2\sqrt{H_0}) + f(v_b)} + g(H_0, v_b)\mathcal{O}(\frac{v_b}{\sqrt{H_0}}) = V_{\rm drift}^0 + V_{\rm drift}^1 \frac{v_b}{\sqrt{H_0}}, \tag{B.3}$$

where $V_{\rm drift}^0 / V_{\rm drift}^1 \sim \mathcal{O}(1)$ for all values of v_b and H_0.

[2]The $v_b \ll 1$ limit corresponds to the case when the barriers are nearly standing. The velocity of the barrier becomes a negligible factor in determining whether the particle crosses or does not cross it, therefore the problem is more symmetric (see Eq. (2.4)). The asymmetry parameters indeed vanish in this limit.

References

[1] H. Poincarè, *Les Mèthods Nouvelles de la Mèchanique Celeste* (Gauthier-Villars, Paris, 1892). [*N.A.S.A. Translation TT F-450/452* (U.S. Fed. Clearinghouse, Springfield, VA, 1967).]

[2] E. N. Lorenz, *J. Atmos. Sci.* **20**, 130 (1963).

[3] H. G. Schuster, *Deterministic Chaos* (Physik-Verlag, Weinheim, 1984).

[4] R. P. Fyenman, R. B. Leighton and M. Sands, *The Feynman Lectures on Physics*, Vol.1, Chaps. 44, 46 (Addisom-Wesley, Reading, MA, 1966).

[5] M. O. Magnasco, *Phys. Rev. Lett.* **71**, 1477 (1993).

[6] R. D. Astumian and M. Bier, *Phys. Rev. Lett.* **72**, 1766 (1993).

[7] J. Prost, J. F. Chauvin, L. Peliti and A. Ajdari, *Phys. Rev. Lett.* **72**, 2652 (1994).

[8] A. Ajdari, D. Mukamel, L. Peliti and J. Prost, *J. Phys. 1 (France)* **4**, 1551 (1994).

[9] J. F. Chauwin, A. Ajdari and J. Prost, *Europhys. Lett.* **27**, 421 (1994).

[10] J. F. Chauwin, A. Ajdari and J. Prost, *Europhys. Lett.* **32**, 373 (1995).

[11] L. P. Faucheux, L.S. Bourdieu, P.D. Kaplan and A.J. Libchaber, *Phys. Rev. Lett.* **74**, 1504 (1995).

[12] L. Gorre, E. Ioannidis and P. Silberzan, *Europhys. Lett.* **33**, 267 (1996).

[13] M. A. Lieberman and A. J. Lichtenberg, *Phys. Rev. A* **5**, 1852 (1972).

[14] G. M. Zaslavskii and B. V. Chirkov, *Dokl. Akad. Nauk SSSR* **159**, 306 (1964). [*Sov. Phys. Dokl.* **9**, 989 (1965).]

[15] A. Brahic, *Astron. and Astrophys.* **12**, 98 (1971).

[16] E. Fermi, *Phys. Rev.* **75**, 1169 (1949).

[17] S. Ulam, in *Proceedings of the Fourth Berkeley Symposium on Mathematics, Statistics and Probability*, Vol. 3, p. 315 (California U. P. , Berkeley, 1961).

[18] A. J. Lichtenberg and M. A. Lieberman, *Regular and Stochastic Motion* (Springer, New York, 1983).

[19] V. I. Arnold and A. Avez, *Ergodic Problems of Classical Mechanics* (Benjamin, New York, 1968).

[20] A. N. Kolmogorov, *Dokl. Akad. Nauk USSR* **98**, 527 (1954).

[21] V. I. Arnold, *Dokl. Akad. Nauk SSSR* **138**, 13 (1961). [*Sov. Math. Dokl.* **2**, 501 (1961).]

[22] V. I. Arnold, *Dokl. Akad. Nauk SSSR* **142**, 758 (1962). [*Sov. Math. Dokl.* **3**, 136 (1962).]

[23] V. I. Arnold, *Dokl. Akad. Nauk SSSR* **145**, 487 (1962). [*Sov. Math. Dokl.* **3**, 1008 (1962).]

[24] J. Moser, *On Invariant Curves of Area-Preserving Mappings on an Annulus.*, Nachr. Akad. Wiss. Gottingen, Math. Phys. K.1, p. 1 (1962).

[25] D. E. Knuth, *The Art of Computer Programming*, Vol. 2 in Seminumerical Algorithms (Addison-Wesley, London, 1969).

[26] R. S. Rasband, *Chaotic Dynamics of Nonlinear Systems* (Wiley-Interscience, New-York, 1990).

[27] L. E. Reichl, *The Transition to Chaos* (Springer-Verlag, New-York, 1992).

TEL AVIV UNIVERSITY
RAYMOND AND BEVERLY SACKLER
FACULTY OF EXACT SCIENCES
SCHOOL OF PHYSICS & ASTRONOMY

אוניברסיטת תל-אביב
הפקולטה למדעים מדוייקים
ע"ש ריימונד ובברלי סאקלר
בית הספר לפיסיקה ואסטרונומיה

תנועה סטוכסטית מכוונת

חיבור זה מוגש כחלק מן הדרישות לקבלת תואר "מוסמך למדעים" M.Sc.

בית הספר לפיסיקה ואסטרונומיה

אוניברסיטת תל–אביב

על–ידי

עודד פרגו

העבודה הוכנה בהדרכתו של פרופסור יעקב קנטור

מאי 1996